EarthArXiv Cover Sheet

Title

Timescale-dependent response of vegetation to climate change

Authors

David Fastovich[1], Stephen R. Meyers[2], Erin E. Saupe[3], John W. Williams[4], Maria Dornelas[5,6], Elizabeth M. Dowding[10], Seth Finnegan[8], Huai-Hsuan M. Huang[9], Lukas Jonkers[10], Wolfgang Kiessling[7], Ádám T. Kocsis[7], Qijian Li[11], Lee Hsiang Liow[12], Lin Na[11], Amelia M. Penny[13], Kate Pippenger[14], Johan Renaudie[15], Marina C. Rillo[16], Jansen Smith[17], Manuel J. Steinbauer[18], Mauro Sugawara[19,20], Adam Tomašovỳch[21], Moriaki Yasuhara[22,23], Pincelli M. Hull[14,24,25]

Affiliations

[1]Department of Earth and Environmental Sciences, Syracuse University, Syracuse, NY, USA
[2]Department of Geoscience, University of Wisconsin – Madison, Madison, WI 53706, USA
[3]Department of Earth Sciences, University of Oxford, South Parks Road, Oxford, OX1 3AN, United Kingdom
[4]Department of Geography & Center for Climatic Research, University of Wisconsin-Madison, 550 N. Park Street, Madison, WI 53706 USA
[5]Department of Earth and Planetary Sciences, Yale University, 210 Whitney Ave, New Haven, CT 06511, USA
[5]University of St Andrews, St. Andrews, United Kingdom
[6]Guia Marine Lab, MARE, Faculty of Science of the University of Lisbon, 939, Estrada do Guincho, Cascais 2750-374, Portugal
[7]GeoZentrum Nordbayern, Friedrich-Alexander Universität Erlangen-Nürnberg (FAU), Erlangen, Germany
[8]Department of Integrative Biology & Museum of Paleontology, University of California, Berkeley, Berkeley, CA USA
[9]Department of Geosciences, Princeton University, NJ, USA
[10]MARUM – Center for Marine Environmental Sciences University of Bremen, Bremen, Germany
[11]State Key Laboratory of Palaeobiology and Stratigraphy, Nanjing Institute of Geology and Palaeontology and Center for Excellence in Life and Paleoenvironment, Chinese Academy of Sciences, Nanjing, China
[12]Natural History Museum & Centre for Planetary Habitability, Department of Geosciences, University of Oslo, Oslo, Norway
[13]School of GeoSciences, University of Edinburgh, Edinburgh, United Kingdom
[14]Department of Earth and Planetary Sciences, Yale University, New Haven, CT, USA
[15]Museum für Naturkunde, Invalidenstraße 43, Berlin, Germany
[16]ICBM - Institute for Chemistry and Biology of the Marine Environment, University of Oldenburg, Wilhelmshaven, Germany
[17]Department of Earth & Environmental Sciences, University of Minnesota - Duluth, Duluth, MN, USA

[18]Bayreuth Center of Ecology and Environmental Research, University of Bayreuth, Bayreuth, Germany
[19]University of British Columbia, Vancouver, BC, Canada
[20]Mário Schenberg Institute, São Paulo, Brazil
[21]Earth Science Institute, Slovak Academy of Sciences, Bratislava, Slovakia
[22]School of Biological Sciences, Area of Ecology and Biodiversity, Swire Institute of Marine Science, Institute for Climate and Carbon Neutrality, Musketeers Foundation Institute of Data Science, The University of Hong Kong, Hong Kong, China
[23]State Key Laboratory of Marine Pollution, City University of Hong Kong, Hong Kong, China
[24]Yale Peabody Museum, 170 Whitney Ave, New Haven, CT, 06511, USA
[25]Swiss Federal Institute for Forest, Snow and Landscape Research, Birmensdorf, Switzerland

Corresponding Author

David Fastovich, dfastovi@syr.edu

Peer-review Statement

This manuscript has been submitted to *Science* and is not peer-reviewed. This preprint has been submitted to EarthArXiv. Subsequent versions of this manuscript may have slightly different content. If accepted, the final version of this manuscript will be available via the 'Peer-reviewed Publication DOI' link on the right-hand side of this webpage.

Title

Timescale-dependent response of vegetation to climate change

Authors

David Fastovich*[1]
Stephen R. Meyers[2]
Erin E. Saupe[3]
John W. Williams[4]
Maria Dornelas[5,6]
Elizabeth M. Dowding[10]
Seth Finnegan[8,9]
Huai-Hsuan M. Huang[10]
Lukas Jonkers[11]
Wolfgang Kiessling[7]
Ádám T. Kocsis[7]
Qijian Li[12]
Lee Hsiang Liow[13]
Lin Na[12]
Amelia M. Penny[14]
Kate Pippenger[15]
Johan Renaudie[16]
Marina C. Rillo[17]
Jansen Smith[18]
Manuel J. Steinbauer[19]
Mauro Sugawara[20,21]
Adam Tomašovỳch[22]
Moriaki Yasuhara[23,24]
Pincelli M. Hull[15,25,26]

*Corresponding Author: dfastovi@syr.edu
[1]Department of Earth and Environmental Sciences, Syracuse University, Syracuse, NY, USA
[2]Department of Geoscience, University of Wisconsin – Madison, Madison, WI 53706, USA
[3]Department of Earth Sciences, University of Oxford, South Parks Road, Oxford, OX1 3AN, United Kingdom
[4]Department of Geography & Center for Climatic Research, University of Wisconsin-Madison, 550 N. Park Street, Madison, WI 53706 USA
[5]Department of Earth and Planetary Sciences, Yale University, 210 Whitney Ave, New Haven, CT 06511, USA
[5]University of St Andrews, St. Andrews, United Kingdom
[6]Guia Marine Lab, MARE, Faculty of Science of the University of Lisbon, 939, Estrada do Guincho, Cascais 2750-374, Portugal
[7]GeoZentrum Nordbayern, Friedrich-Alexander Universität Erlangen-Nürnberg (FAU), Erlangen, Germany

[8]Department of Integrative Biology & Museum of Paleontology, University of California, Berkeley, Berkeley, CA USA
[9]Smithsonian Tropical Research Institute, Panama
[10]Department of Geosciences, Princeton University, NJ, USA
[11]MARUM – Center for Marine Environmental Sciences University of Bremen, Bremen, Germany
[12]State Key Laboratory of Palaeobiology and Stratigraphy, Nanjing Institute of Geology and Palaeontology and Center for Excellence in Life and Paleoenvironment, Chinese Academy of Sciences, Nanjing, China
[13]Natural History Museum & Centre for Planetary Habitability, Department of Geosciences, University of Oslo, Oslo, Norway
[14]School of GeoSciences, University of Edinburgh, Edinburgh, United Kingdom
[15]Department of Earth and Planetary Sciences, Yale University, New Haven, CT, USA
[16]Museum für Naturkunde, Invalidenstraße 43, Berlin, Germany
[17]ICBM - Institute for Chemistry and Biology of the Marine Environment, University of Oldenburg, Wilhelmshaven, Germany
[18]Department of Earth & Environmental Sciences, University of Minnesota - Duluth, Duluth, MN, USA
[19]Bayreuth Center of Ecology and Environmental Research, University of Bayreuth, Bayreuth, Germany
[20]University of British Columbia, Vancouver, BC, Canada
[21]Mário Schenberg Institute, São Paulo, Brazil
[22]Earth Science Institute, Slovak Academy of Sciences, Bratislava, Slovakia
[23]School of Biological Sciences, Area of Ecology and Biodiversity, Swire Institute of Marine Science, Institute for Climate and Carbon Neutrality, Musketeers Foundation Institute of Data Science, The University of Hong Kong, Hong Kong, China
[24]State Key Laboratory of Marine Pollution, City University of Hong Kong, Hong Kong, China
[25]Yale Peabody Museum, 170 Whitney Ave, New Haven, CT, 06511, USA
[26]Swiss Federal Institute for Forest, Snow and Landscape Research, Birmensdorf, Switzerland

Abstract

Climate and ecosystems exhibit dynamic behavior across various timescales, but existing studies often focus on singular timescales when examining ecosystem responses to climate. Here we develop a conceptual and analytical framework using spectral analysis that examines a continuum of timescales, from hundreds to hundreds of thousands of years. By comparing power spectra of vegetation turnover and climate in the last 1.1 million years, we observe that turnover is in step with climate at intermediate frequencies (10^{-2} to 10^{-3} $years^{-1}$) but is decoupled from climate at high frequencies (> 10^{-2} $years^{-1}$) and low frequencies (<10^{-3} $years^{-1}$), with a relationship that varies by latitude. Climate decoupling at the highest frequencies highlights the possibility of widespread ecological transitions in the coming century as anthropogenic climate change outpaces the response time of plant communities.

Keywords

Spectral power continuum, community turnover, climate variability, dynamic equilibrium, non-linear ecological dynamics, temporal beta diversity, vegetation

Manuscript Text

The biosphere is a dynamic component of the Earth system that is sensitive to climate variability, with eco-evolutionary processes operating across a broad range of timescales (*1–3*). Ecologists have long recognized that species and ecological systems differ in their responses to changing climates, and that these dynamics are timescale dependent (*3–6*). However, most studies of climate-driven ecological dynamics have focused on narrow ranges of timescales , leaving critical gaps in our understanding of how communities respond to environmental change across the continuous range of timescales experienced by biota (*7*, *8*).

With recent advances in the characterization of climate variability across timescales (*9*, *10*) and the growth of global networks of ecological, paleoecological, and paleobiological data resources across timescales (*11*, *12*), we can now more fully characterize the timescales at which ecological systems are characterized by fast, slow, and/or nonlinear responses to climatic forcing. Fast ecological dynamics can track climate change (*13*, *14*), while slow dynamics are lagged or decoupled from climate (*15–18*). In addition, ecosystems can linearly or nonlinearly respond to forcing (e.g. (*19*)), with the potential for nonlinear responses to lead to abrupt compositional changes or other ecological regime shifts (*20*). Characterizing the nature of dynamics across time scales is urgently required for understanding how and at what rates ecological systems are likely to respond to anthropogenic climate change (*21*).

Here, we focus on the relationship between temperature, precipitation, and vegetation compositional turnover in time series spanning hundreds to hundreds of thousands of years for the last 1.1 million years, with densest coverage for the last 20,000 years. Across these timescales, the drivers of vegetation compositional change vary in their relative importance (Fig. 1): disturbance, biotic interactions, and demographic processes are thought to be more important at shorter timescales; dispersal limitation, population dynamics, and ecosystem transformation dominate at intermediate timescale; and macroevolutionary processes such as speciation and extinction prevail at longer timescales (*1*, *2*).

To study the relationship between timescales of climate variability and vegetation dynamics, we develop and apply a conceptual and analytical framework rooted in spectral analysis (*22*), widely used in climate science (*9*, *23–25*). We generate global power spectra of community dynamics by averaging site-level power spectra for fossil pollen assemblages from a global compilation of 1,250 sites. We compare global vegetation compositional change from the empirical records with the global power spectra of temperature and precipitation from a climate simulation of the last 21,000 years (TraCE-21ka) (*26*, *27*). To mirror the sedimentation process and sample coverage of the pollen timeseries, climate simulations were low-pass filtered (*28*) and spatiotemporally downsampled. To capture lower-frequency climate variability on durations longer than the TraCE-21ka model simulation, we include proxy climate reconstructions that approximate global climate from EPICA Dome C (*29*) and a proxy-based reconstruction of global surface air temperature of the last two million years (*30*). By comparing the global dynamics of climate and

vegetation across timescales we assess the response of plant communities across temporal scales to climate variability.

Paired Spectral Analysis of Climate and Vegetation: Analytical and Conceptual Framework

Paired spectral analyses of climate and ecological timeseries allow us to quantify the relationship between climate variability and community turnover across timescales (*31*, *32*). The relationship between the climate system and vegetation composition can be assessed in frequency space by comparing the spectral continuum of variability in vegetation turnover to variability in climate. For many physical systems, the exponential coefficient of the power-law relationship (β in $S(f) \propto f^{-\beta}$) between spectral power (S) and frequency (f) defines the spectral continuum. Within a time series, β characterizes memory (i.e. temporal autocorrelation) and how variance is partitioned across timescales (*25*). If the exponential coefficient (β) of the power-law relationship between frequency and spectral power is small ($\beta \sim 0$), variance is equally partitioned among all frequencies (Fig. S1) (*25*). In contrast, $\beta > 0$ indicates more variance at lower frequencies (longer periods), with $\beta = 2$ defining a random walk (Fig. S1) (*25*).

In the climate system, short-lived, stochastic, weather processes interact within the Earth system and scale into climate processes that possess increasing variability with decreasing frequency (*33*). These two modes of climate variability emerge as distinct βs for high (low β) and low frequencies (high β), with a break between 100^{-1} to $1{,}000^{-1}$ $years^{-1}$ (*9*, *10*).

If vegetation can dynamically track changes in climate on frequencies smaller than 100^{-1} to $1{,}000^{-1}$ $years^{-1}$ (*13*, *14*), then the spectral continuum for vegetation turnover and climate is expected to be similar, with similar βs and perhaps containing a scaling break similar to that observed for the climate system (Fig. 1A, $\beta_{veg} = \beta_{clim}$).We expect that fast tracking of climate change by ecological communities is more likely to emerge at millennial to orbital timescales (roughly 1,000 to 100,000 years), where plant communities are influenced by ecological and biogeographic processes such as environmental filtering, dispersal, and local population extirpation (Fig. 1). At these intermediate timescales, the processes determining community composition, such as dispersal and ecosystem transformations caused by changing species' abundances, act quickly relative to the pacing of climate variability. Many prior studies have used fossil pollen records and other micropaleontological records as indicators of past climates at these timescales (*34–37*), grounded in theoretical expectations that ecological dynamics are well approximated by dynamic ecological equilibrium with climate oscillations (*13*).

However, the relationship between climate and vegetation dynamics at longer and shorter timescales remains an open question (Fig. 1). Shorter timescales (hundreds of years) are particularly crucial for predicting vegetation responses to anthropogenic climate warming, as they allow exploration of how plant ecology and life-history factors may override the influence of climate variability. Trees tend to be long-lived organisms (*38*) and can outlive short-term climate variability within their physiological tolerance limits. Consequently, ecological variability would be low at the highest frequencies but high at the frequencies corresponding with tree senescence. This contrasts with the climate system where variance is equally partitioned among all frequencies in the weather regime. In frequency space, this would manifest

as a larger β in vegetation than in climate (Fig. 1B, $\beta_{veg} > \beta_{clim}$). Conversely, disturbance through herbivory, fire, human land use, and disease could produce an opposite signal by increasing vegetation turnover at high frequencies thereby causing a smaller β relative to the climate power spectrum (Fig. 1B, $\beta_{veg} < \beta_{clim}$).

At the longest timescales, climate tracking could persist, as expected at intermediate timescales (Fig. 1C, $\beta_{veg} = \beta_{clim}$). Alternatively, adaptive evolution could increase species' tolerances to new climate regimes (*39*), potentially reducing community compositional responses to climate forcing and species' sensitivity to environmental changes. As a product of compositional stability, ecological variability would increase minimally as frequencies decrease (increasing timescales) relative to climate variations. (Fig. 1C, $\beta_{veg} < \beta_{clim}$). Conversely, if ecological systems are characterized by strong non-linearities in ecological response to environmental forcings (*40–42*), ecological turnover would be high relative to climate forcings and ecological variability would increase as frequency decreases at a greater rate than climate variability (Fig. 1C, $\beta_{veg} > \beta_{clim}$). As in the climate system, the timescales at which these alternative processes operate are identifiable as breakpoints in β.

Spectral continuum of vegetation variability

To minimize sampling effects when comparing the power spectrum of pollen variability to that of climate variability, we downsample and low-pass filter the simulated climate time series from TraCE-21ka to match the spatiotemporal characteristics of the fossil pollen archives (see Methods). However, the pollen and climate proxy data (EPICA Dome C, S16 GAST) have different spatiotemporal characteristics. We assess the effects of temporal uncertainty and uneven spatiotemporal coverage of the fossil pollen data by resampling sites and their corresponding posterior age estimates to produce an ensemble of power spectra, estimates of β, and estimates of the breakpoints in β (see Methods).

We find that the spectral continuum of variability in pollen carries clear similarities to that of the climate system (Fig. 2), yet the relationship to climate varies with timescale. Unlike temperature and precipitation in our analyses (Fig. 2) or in previous studies (*9*, *10*, *23*, *43*), the fossil pollen power spectra have three breakpoints, determined using segmented regressions (*44*), at 152^{-1} $years^{-1}$, 872^{-1} $years^{-1}$, and $4{,}789^{-1}$ $years^{-1}$ (uncertainties for all parameters estimated are reported in Table S1). The fossil pollen power spectra are therefore characterized by four characteristic timescales: high frequencies ($< 152^{-1}$ $years^{-1}$); high-intermediate frequencies (152^{-1} to 872^{-1} $years^{-1}$); low-intermediate frequencies (872^{-1} to $4{,}789^{-1}$ $years^{-1}$); and low frequencies ($> 4{,}789^{-1}$ $years^{-1}$). This pattern contrasts with the characteristic timescales found for temperature and precipitation, which have only two characteristic timescales with single breakpoints at 625^{-1} and 635^{-1} $years^{-1}$, respectively, similar to prior studies (*10*). The presence of additional breakpoints in β in the fossil pollen power spectra found in the full ensemble (Fig. 1) are also found in our best-resolved individual records (Fig. S2), indicating the patterns are not an artifact of the ensemble approach. Together, these features of the fossil pollen power spectra provide striking evidence that the relationship between plant communities and climate is timescale-dependent and complex. Ecological communities and climate may co-vary on some timescales but differ in their dynamics on others.

Timescales of Ecological Dynamics

Tracking of climate change by ecological systems is indicated across the intermediate frequencies of 152^{-1} to $4{,}789^{-1}$ $years^{-1}$ (Fig. 2), where the continuum of fossil pollen turnover and climate variability have similar βs. Specifically, βs are near zero at high intermediate frequencies of 152^{-1} to 872^{-1}years, and ~2-3 at low intermediate frequencies of 872^{-1} to $4{,}789^{-1}$ $years^{-1}$. In these two intermediate frequency regimes, centennial to millennial-scale climate variation is characterized by changes in temperature and precipitation (*45*, *46*). Temperature and precipitation, in turn, have been identified as the primary correlates of pollen assemblage turnover on the same timescales (*47–51*). It is generally thought that rapid changes in local abundances, which are relatively fast compared to millennial-scale climate variability (*48*), allow plant communities to dynamically adjust composition and structure in response to climate forcing on these timescales (*13*, *14*). This pattern emerges in our results as similar βs for climate and vegetation in frequency space.

Vegetation in the intermediate frequency regime appears to follow the climate system across the weather-climate breakpoint (631^{-1}—567^{-1} $years^{-1}$ for temperature; 639^{-1}—631^{-1} $years^{-1}$ for precipitation; 881^{-1}—857^{-1} $years^{-1}$ for pollen), supporting the interpretation that vegetation dynamically tracks the climate system across the intermediate frequency regime. Although the breakpoint for pollen is statistically distinguishable from that of temperature and precipitation (i.e., non-overlapping 95% confidence bounds on breakpoint placement), the different breakpoints may be more apparent, rather than real. The non-random subset of communities recorded by these fossil pollen records, our choice of climate model, or biased local/regional spectral estimates from climate models (*43*, *52*) all likely contribute to this apparent difference in breakpoints. However, if this offset between the vegetation and climate breakpoints is real rather than an artifact, two hypotheses may explain the brief decoupling of climate and vegetation between frequencies of 639^{-1}—567^{-1} $years^{-1}$ and 872^{-1} $years^{-1}$: a lag in vegetation response to the transition from low, β weather to higher β, climate regimes or the greater importance of non-climatic forcing (such as disturbance regimes) on these timescales.

Unlike the intermediate frequency regime, the high and low frequency regimes exhibit climate decoupling. β is nearly two for pollen at the shortest, high-frequency timescales (< 152^{-1} $years^{-1}$, 3.51 95% CI: 3.14, 3.81), while for temperature and precipitation the β is -0.15 (-0.19, -0.11) and -0.61 (-0.63, -0.57), respectively (Fig. 2). This finding supports prior observations of higher βs in vegetation assemblages at these short timescales (*53*) but appears sensitive to the amount of weight given to abundant and rare taxa in the dissimilarity metric and the pollen record under consideration (Fig. S3). Both taphonomic and ecological processes could explain higher βs in the pollen data in some sites and metrics. Decadal-scale mixing of lake sediments (*54*), scale gaps caused by discontinuous sampling of sediment cores (*12*), and variable preservation may enhance autoregressive correlation in these archives (*28*). Alternatively, or in addition, the relatively large βs at the shortest timescales may be due to the longer life spans of some plants (e.g. trees), limiting the ability of the full community to track climate due to slow turnover times (*53*). Indeed, the median tree lifespan from the International Tree Ring Data Bank (*55*, *56*) is 246 years (n = 4,773) (Fig. S4). Finally, a greater β for fossil pollen assemblages at the highest frequencies is consistent with observations of slow ecological response to climate variability and evidence of climate debt at these timescales (*16–18*, *57*).

In the low-frequency regime (timescales longer than $4{,}789^{-1}$ years), we observe βs of 0.83 (0.81, 0.84) for fossil pollen power spectra (Fig. 2). A low β for vegetation in the low frequency regime contrasts the climate power spectra, which maintain the long-term climate system βs of ~2-3 due to the influence of astronomical forcing of ice sheets (Fig. 2) (*58*, *59*). There are two possible explanations for low βs in pollen at these longer timescales. First, low pollen βs may reflect the saturation of community dissimilarity metrics used to compare pollen assemblages across the time series (Fig. S5), resulting in an apparent decrease in the rate of community turnover as timescale increases even if the absolute amount of community change remained the same. The other potential explanation for the low βs at frequencies below $4{,}789^{-1}$ $years^{-1}$ is fast evolutionary adaptation by species to environmental variation that results in pollen communities appearing relatively resistant to climate forcing. Although local adaptation cannot be excluded, the hypothesis of metric saturation appears sufficient to explain the reduced pollen variability at longer timescales.

Non-Linearity in the Climate-Vegetation Relationship

The pollen power spectrum is characterized by a breakpoint at $4{,}789^{-1}$ $years^{-1}$, which is absent in the power spectra of climate proxies and climate simulations (Fig. 2) (*9*, *10*). The community dissimilarity metrics we used record the emergence of largely dissimilar communities at multimillennial timescales. Metrics that more evenly weigh abundant and rare taxa providing the clearest representation of the $4{,}789^{-1}$ $year^{-1}$ breakpoint and low β for the low frequency regime that follows (Fig. S3). This breakpoint might emerge here, rather than another interval, because many contemporary plant communities in eastern North America originated during the Holocene, with several ecosystem transformations during the past 11,000 years (*60*). Paleoclimate proxies in the North Atlantic have been argued to contain an apparent mode of climate variability at $1{,}470^{-1}$ and $4{,}670^{-1}$ $years^{-1}$ (*61*), and provide a plausible mechanism for forcing vegetation turnover (*35*, *48*, *62*). However, global compilations of Holocene climate records lack high spectral power at any of these frequencies (*63*), as do our power spectra of temperature and precipitation (Fig. 2). This disconnect at the global scale, and in the subset of sites we investigated, between climate and pollen lead us to hypothesize that relatively subtle or regional millennial-scale climate variations may be amplified in the vegetation signal by non-linear ecological dynamics (*40*, *42*).

However, analytical artifacts could lead or contribute to the breakpoint at $4{,}789^{-1}$ $years^{-1}$. Most of our records span the last 20,000 years with just a few long records exceeding that duration (Fig. S6). The change in the set of sites being averaged could contribute to a shift in the ecological dynamics and β with longer time scales, with the relatively low number of sites sampled biasing our spatial and environmental coverage at low frequencies. Regardless, the behavior of vegetation community dynamics over the last 1.1 million years provides a foundation for considering the influence of nonlinear dynamics on millennial timescales and underscores the potential for abrupt changes in plant communities over the coming decades of warming (*64*, *65*).

Latitudinal Gradient in Community Dynamics

We find that the relationship between plant community variability and climate variability differs across latitudes. Climatically, the high latitudes experience greater temperature variability than the tropics across all timescales, while the tropics experience greater precipitation variability (Fig. 3) (*9*). Fossil pollen turnover appears to resemble temperature, in that tropical sites (< 23.5°) have less vegetation variability than extra-tropical sites (> 23.5°), although the power spectra have overlapping confidence bounds across most of frequency space (Fig. 3A). This overlap is caused mostly by larger differences among tropical fossil pollen power spectra. At frequencies of 871^{-1} – $4{,}732^{-1}$ years^{-1}, extra-tropical sites have a β of 2.92 that match those of temperature and precipitation, while tropical sites appear to have a β of 1.83, but with high uncertainty (Fig. 3). Thus, there is the possibility that tropical fossil pollen communities are less sensitive to climate forcing across the timescales investigated, are affected more by non-climatic factors, or are more stable and resistant to turnover. On modern timescales, other studies have reported that net primary production in the low latitudes is relatively sensitive to solar radiation and precipitation, in contrast to higher sensitivity to temperature in the high northern latitudes (*66*).

Conclusions

Our framework to establish a global relationship between plant community turnover and climate variability over frequencies ranging from 100^{-1} to 100,000 years^{-1} revealed a non-linear and timescale-dependent relationship between vegetation and climate variability. At timescales of 152^{-1}- $4{,}789^{-1}$ years, we see evidence for vegetation tracking of climate change. The disconnect in the scaling of variability in the climate system and pollen assemblages at timescales shorter than 152 years could be due to sediment processes but also reinforces concerns that biotic processes will be slow to respond to contemporary climate warming and changing climate variability (*15*). Consequently, the fast rate of anthropogenic climate change may outstrip the response time of plant communities (*21*) leading to delayed and widespread ecological transitions (*67*) that challenge predicting vegetation responses to current warming.

Acknowledgements

This project is a contribution to the BioDeepTime project, supported by Paleosynthesis Project, which is funded by the Volkswagen Foundation (Az 96 796). D.F. acknowledges postdoctoral support from NSF OCE-2103015, NSF AGS-2402498, and the College of Arts and Sciences at Syracuse University. We are grateful to Yasuhiro Kubota for convening the P-SEEDS workshop where the idea for this project began. Many thanks to the Syracuse University High Throughput Computing Campus Grid (OrangeGrid) for providing computational resources and to Jon Cheney for technical support. Funding for OrangeGrid is provided by ACI-1341006. EES acknowledges support from a Leverhulme Prize and NERC grant NE/V011405/1. L.J. is supported through the German climate modeling initiative PALMOD, funded by the German Ministry of Science and Education (BMBF, 01LP1922A). PMH acknowledges sabbatical support from the Swiss Federal Institute for Forest, Snow and Landscape Research. Fossil pollen data were obtained from the Neotoma Paleoecology Database (http://www.neotomadb.org) and its constituent databases: the African Pollen Database, European Pollen Database, Indo-Pacific Pollen Database, Latin American Pollen Database, and North American Pollen Database. The

work of data contributors, data stewards, and the Neotoma community is gratefully acknowledged.

Data Availability Statement

Data and code needed to reproduce all analyses are available on Zenodo (*68*).

Author Contributions

DF and PMH developed the research questions and study design. DF, SRM, EES, JWW, and PMH co-developed the theoretical framework. DF performed all analyses with help from SRM and EES. DF led writing with support from SRM, EES, JWW, and PMH. The ideas for this paper originated from discussions by the BioDeepTime working group. All authors reviewed and contributed to the article.

Figures

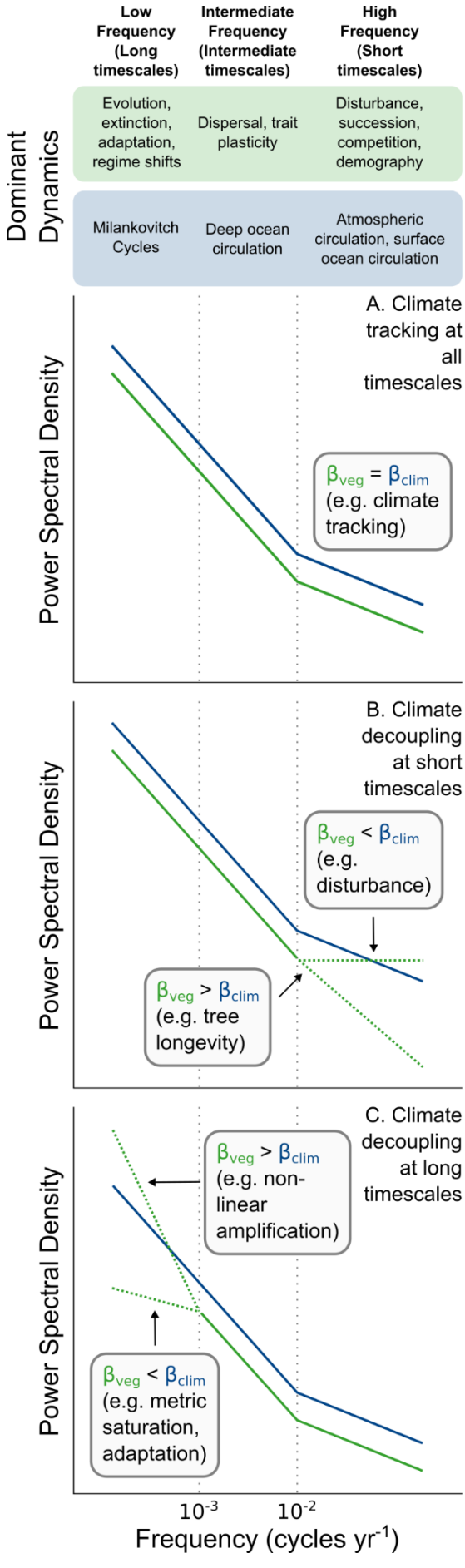
Low Frequency (Long timescales)
Intermediate Frequency (Intermediate timescales)
High Frequency (Short timescales)
Dominant Dynamics
Evolution, extinction, adaptation, regime shifts
Dispersal, trait plasticity
Disturbance, succession, competition, demography
Milankovitch Cycles
Deep ocean circulation
Atmospheric circulation, surface ocean circulation
A. Climate tracking at all timescales
Power Spectral Density
βveg = βclim (e.g. climate tracking)
B. Climate decoupling at short timescales
βveg < βclim (e.g. disturbance)
βveg > βclim (e.g. tree longevity)
C. Climate decoupling at long timescales
βveg > βclim (e.g. non-linear amplification)
βveg < βclim (e.g. metric saturation, adaptation)
10-3
10-2
Frequency (cycles yr-1)

Figure 1. A conceptual framework for interpreting the relationship between vegetation and climate using power spectra through the power-law scaling relationship between spectral power and frequency ($S(f) \propto f^{-\beta}$). The blue line corresponds to β for climate variability and the green line corresponds to β for vegetation compositional turnover. The breakpoint in climate spectral power in all three panels is based on prior work that indicates a breakpoint in climate variability at approximately 100^{-1} $years^{-1}$ (*9*). Key phenomena include the slope (β, i.e. continuum) of vegetation turnover relative to climate and the placement of breakpoints. Three scenarios illustrate potential relationships between climate and vegetation. (A) Vegetation composition exhibits fast and linear responses to climate across all frequencies and so the slope of vegetation spectral power parallels that of climate. (B) Vegetation quickly and linearly tracks climate at intermediate frequencies and low frequencies (*13*), but is decoupled from climate at high frequencies. A higher β for vegetation turnover than climate suggests that processes such as tree longevity influence high frequency vegetation turnover while a lower β for vegetation indicates that disturbance may be a primary control on high frequency vegetation turnover. (C) Vegetation tracks climate across high and intermediate frequencies but is decoupled at low frequencies from processes like evolutionary adaptation (lower β for vegetation) or non-linear amplification through processes such as threshold responses (higher β for vegetation). Other scenarios and ecological processes are possible beyond those shown here.

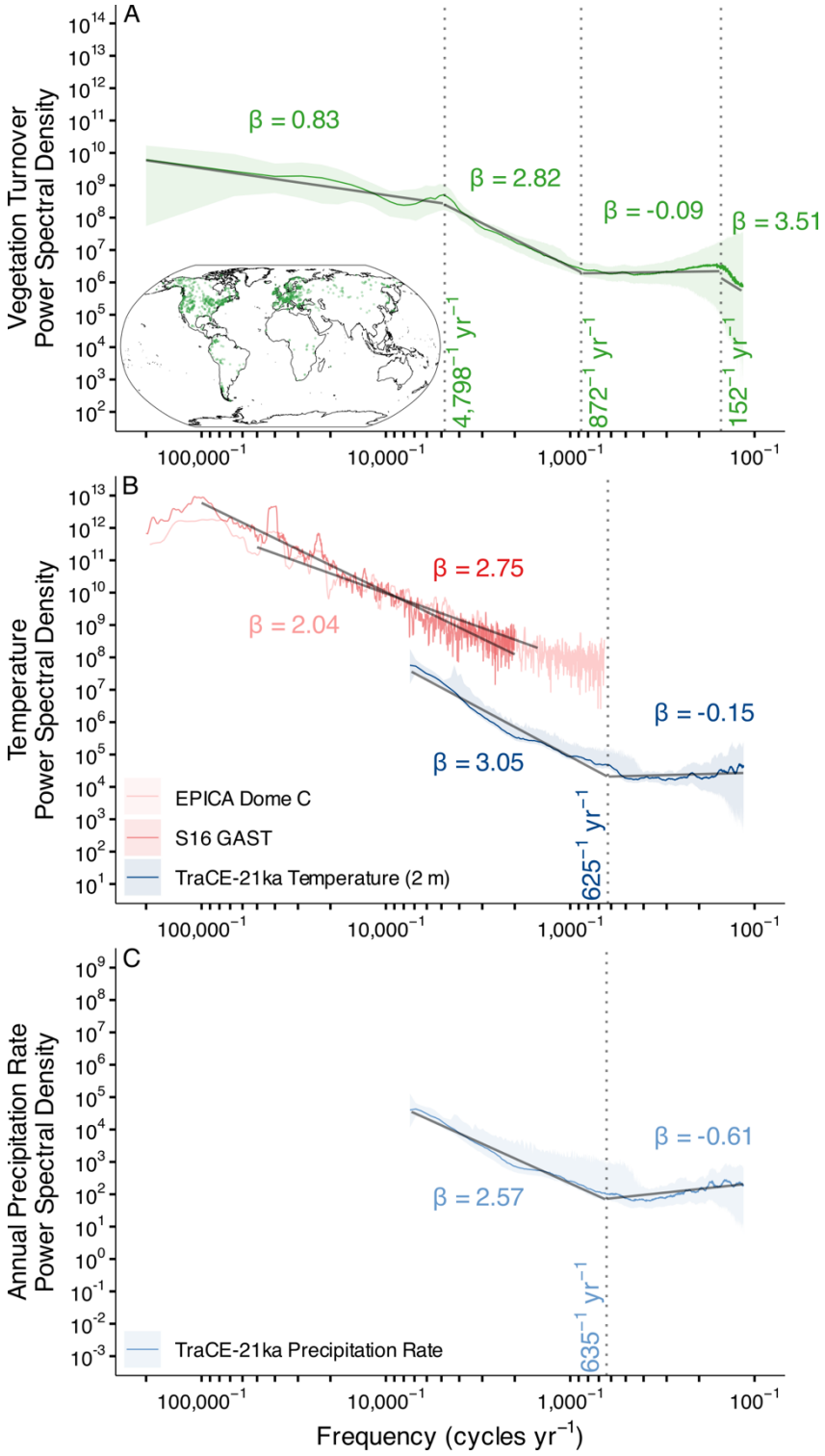

Figure 2. The spectral continuum of (A) vegetation turnover (green), (B) temperature (blue, red, pink), and (C) precipitation (light blue) variability for frequencies with spectral power estimates from a median of two sites across the ensemble of spectral power estimates. Solid gray lines correspond to β from ordinary least squares regressions of log-spectral power and log-frequency. Vertical dashed lines correspond to breakpoints identified in the spectral continuum. Climate estimates from TraCE-21ka have been downsampled in space and time and low-pass filtered to

match the temporal characteristics of the fossil pollen abundances. Uncertainties for β and breakpoints are reported in the Supplementary Information (Table S1).

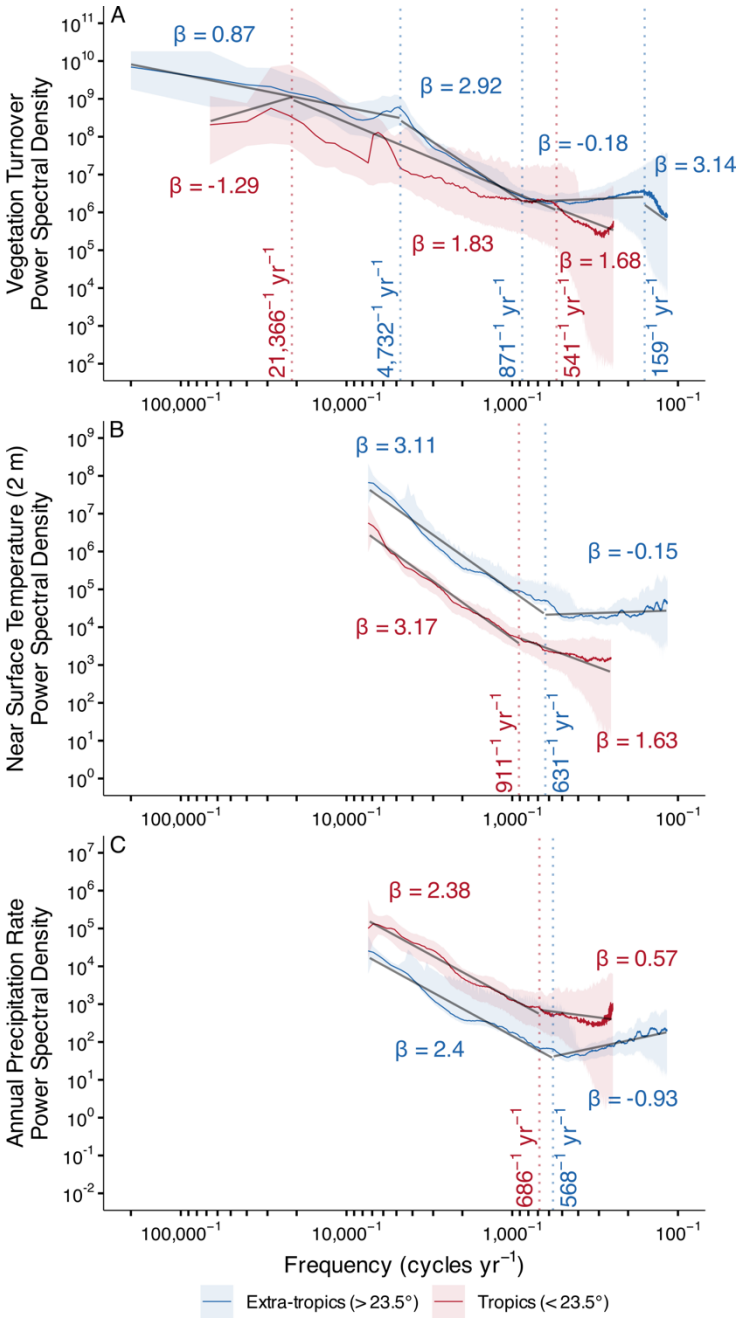

Figure 3. The continuum of (A) vegetation turnover, (B) near surface temperature, and (C) annual precipitation rate variability, averaged for the extra-tropics (blue, > 23.5°) and tropics (red, < 23.5°) for frequencies with spectral power estimates from a median of two sites across the ensemble of spectral power estimates. Vertical dashed lines correspond to breakpoints identified in the spectral continuum and are colored by the corresponding spatial average. All climate estimates are from TraCE-21ka and have been downsampled as in Figure 1. Uncertainties for β and breakpoints are reported in the Supplementary Information (Table S1)

References

1. J. Overpeck, C. Whitlock, B. Huntley, "Terrestrial Biosphere Dynamics in the Climate System: Past and Future" in *Paleoclimate, Global Change and the Future*, K. D. Alverson, T. F. Pedersen, R. S. Bradley, Eds. (Springer, Berlin, Heidelberg, 2003; https://doi.org/10.1007/978-3-642-55828-3_5)*Global Change — The IGBP Series*, pp. 81–103.

2. E. M. Wolkovich, B. I. Cook, K. K. McLauchlan, T. J. Davies, Temporal ecology in the Anthropocene. *Ecology Letters* **17**, 1365–1379 (2014).

3. D. Jablonski, Biotic interactions and macroevolution: extensions and mismatches across scales and levels. *Evolution* **62**, 715–739 (2008).

4. R. E. Ricklefs, Community Diversity: Relative Roles of Local and Regional Processes. *Science* **235**, 167–171 (1987).

5. H. R. Delcourt, P. A. Delcourt, Quaternary landscape ecology: Relevant scales in space and time. *Landscape Ecol* **2**, 23–44 (1988).

6. P. F. McDowell, T. Webb, P. J. Bartlein, "Long-Term Environmental Change" in *Ecological Time Series*, T. M. Powell, J. H. Steele, Eds. (Springer US, Boston, MA, 1995; https://doi.org/10.1007/978-1-4615-1769-6_16), pp. 327–370.

7. A. S. Mori, T. Sasaki, M. Kagami, T. Miki, M. Yasuhara, "Feedbacks Between Biodiversity and Climate Change" in *The Ecological and Societal Consequences of Biodiversity Loss* (John Wiley & Sons, Ltd, 2022; https://onlinelibrary.wiley.com/doi/abs/10.1002/9781119902911.ch13), pp. 281–304.

8. M. Yasuhara, R. Danovaro, Temperature impacts on deep-sea biodiversity. *Biological Reviews* **91**, 275–287 (2016).

9. P. Huybers, W. Curry, Links between annual, Milankovitch and continuum temperature variability. *Nature* **441**, 329–332 (2006).

10. F. Zhu, J. Emile-Geay, N. P. McKay, G. J. Hakim, D. Khider, T. R. Ault, E. J. Steig, S. Dee, J. W. Kirchner, Climate models can correctly simulate the continuum of global-average temperature variability. *Proceedings of the National Academy of Sciences* **116**, 8728–8733 (2019).

11. J. W. Williams, E. C. Grimm, J. L. Blois, D. F. Charles, E. B. Davis, S. J. Goring, R. W. Graham, A. J. Smith, M. Anderson, J. Arroyo-Cabrales, A. C. Ashworth, J. L. Betancourt, B. W. Bills, R. K. Booth, P. I. Buckland, B. B. Curry, T. Giesecke, S. T. Jackson, C. Latorre, J. Nichols, T. Purdum, R. E. Roth, M. Stryker, H. Takahara, The Neotoma Paleoecology Database, a multiproxy, international, community-curated data resource. *Quaternary Research* **89**, 156–177 (2018).

12. J. Smith, M. C. Rillo, Á. T. Kocsis, M. Dornelas, D. Fastovich, H.-H. M. Huang, L. Jonkers, W. Kiessling, Q. Li, L. H. Liow, M. Margulis-Ohnuma, S. Meyers, L. Na, A. M. Penny, K. Pippenger, J. Renaudie, E. E. Saupe, M. J. Steinbauer, M. Sugawara, A. Tomašovỳch, J. W. Williams, M. Yasuhara, S. Finnegan, P. M. Hull, BioDeepTime: A database of biodiversity time series for modern and fossil assemblages. *Global Ecology and Biogeography* **n/a** (2023).

13. T. Webb, Is vegetation in equilibrium with climate? How to interpret late-Quaternary pollen data. *Vegetatio* **67**, 75–91 (1986).

14. J. W. Williams, A. Ordonez, J.-C. Svenning, A unifying framework for studying and managing climate-driven rates of ecological change. *Nat Ecol Evol* **5**, 17–26 (2021).

15. J.-C. Svenning, B. Sandel, Disequilibrium vegetation dynamics under future climate change. *American Journal of Botany* **100**, 1266–1286 (2013).

16. M. V. Talluto, I. Boulangeat, S. Vissault, W. Thuiller, D. Gravel, Extinction debt and colonization credit delay range shifts of eastern North American trees. *Nat Ecol Evol* **1**, 1–6 (2017).

17. R. Bertrand, J. Lenoir, C. Piedallu, G. Riofrío-Dillon, P. de Ruffray, C. Vidal, J.-C. Pierrat, J.-C. Gégout, Changes in plant community composition lag behind climate warming in lowland forests. *Nature* **479**, 517–520 (2011).

18. B. J. Butterfield, R. S. Anderson, C. A. Holmgren, J. L. Betancourt, Extinction debt and delayed colonization have had comparable but unique effects on plant community–climate lags since the Last Glacial Maximum. *Global Ecology and Biogeography* **28**, 1067–1077 (2019).

19. R. Spake, M. P. Barajas-Barbosa, S. A. Blowes, D. E. Bowler, C. T. Callaghan, M. Garbowski, S. D. Jurburg, R. van Klink, L. Korell, E. Ladouceur, R. Rozzi, D. S. Viana, W.-B. Xu, J. M. Chase, Detecting Thresholds of Ecological Change in the Anthropocene. *Annual Review of Environment and Resources* **47**, 797–821 (2022).

20. S. R. Carpenter, O. Kinne, *Regime Shifts in Lake Ecosystems : Pattern and Variation* (Ecology Institute, Oldendorf/Luhe, Germany, 2003)*Excellence in ecology,*.

21. Intergovernmental Panel On Climate Change (Ipcc), *Climate Change 2021 – The Physical Science Basis: Working Group I Contribution to the Sixth Assessment Report of the Intergovernmental Panel on Climate Change* (Cambridge University Press, ed. 1, 2023; https://www.cambridge.org/core/product/identifier/9781009157896/type/book).

22. D. J. Thomson, Spectrum estimation and harmonic analysis. *Proceedings of the IEEE* **70**, 1055–1096 (1982).

23. R. Hébert, U. Herzschuh, T. Laepple, Millennial-scale climate variability over land overprinted by ocean temperature fluctuations. *Nat. Geosci.*, 1–7 (2022).

24. P. Yiou, E. Baert, M. F. Loutre, Spectral analysis of climate data. *Surv Geophys* **17**, 619–663 (1996).

25. C. Wunsch, The spectral description of climate change including the 100 ky energy. *Climate Dynamics* **20**, 353–363 (2003).

26. F. He, *Simulating Transient Climate Evolution of the Last Deglaciation with CCSM 3* (2011)vol. 72.

27. Z. Liu, B. L. Otto-Bliesner, F. He, E. C. Brady, R. Tomas, P. U. Clark, A. E. Carlson, J. Lynch-Stieglitz, W. Curry, E. Brook, D. Erickson, R. Jacob, J. Kutzbach, J. Cheng, Transient Simulation of Last Deglaciation with a New Mechanism for Bølling-Allerød Warming. *Science* **325**, 310–314 (2009).

28. R. Hébert, K. Rehfeld, T. Laepple, Comparing estimation techniques for temporal scaling in palaeoclimate time series. *Nonlinear Processes in Geophysics* **28**, 311–328 (2021).

29. J. Jouzel, V. Masson-Delmotte, O. Cattani, G. Dreyfus, S. Falourd, G. Hoffmann, B. Minster, J. Nouet, J. M. Barnola, J. Chappellaz, H. Fischer, J. C. Gallet, S. Johnsen, M. Leuenberger, L. Loulergue, D. Luethi, H. Oerter, F. Parrenin, G. Raisbeck, D. Raynaud, A. Schilt, J. Schwander, E. Selmo, R. Souchez, R. Spahni, B. Stauffer, J. P. Steffensen, B. Stenni, T. F. Stocker, J. L. Tison, M. Werner, E. W. Wolff, Orbital and Millennial Antarctic Climate Variability over the Past 800,000 Years. *Science* **317**, 793–796 (2007).

30. C. W. Snyder, Evolution of global temperature over the past two million years. *Nature* **538**, 226–228 (2016).

31. T. Platt, K. L. Denman, Spectral Analysis in Ecology. *Annu. Rev. Ecol. Syst.* **6**, 189–210 (1975).

32. M. E. Dillon, H. A. Woods, G. Wang, S. B. Fey, D. A. Vasseur, R. S. Telemeco, K. Marshall, S. Pincebourde, Life in the Frequency Domain: the Biological Impacts of Changes in Climate Variability at Multiple Time Scales. *Integrative and Comparative Biology* **56**, 14–30 (2016).

33. K. Hasselmann, Stochastic climate models Part I. Theory. *Tellus* **28**, 473–485 (1976).

34. M. Chevalier, B. A. S. Davis, O. Heiri, H. Seppa, B. M. Chase, K. Gajewski, T. Lacourse, R. J. Telford, W. Finsinger, J. Guiot, N. Kuhl, S. Y. Maezumi, J. R. Tipton, V. A. Carter, T. Brussel, L. N. Phelps, A. Dawson, M. Zanon, F. Valle, C. Nolan, A. Mauri, A. de Vernal, K. Izumi, L. Holmstrom, J. Marsicek, S. Goring, P. S. Sommer, M. Chaput, D. Kupriyanov, Pollen-based climate reconstruction techniques for late Quaternary studies. *Earth-Sci. Rev.* **210**, 33 (2020).

35. D. Fastovich, J. M. Russell, S. T. Jackson, T. R. Krause, S. A. Marcott, J. W. Williams, Spatial fingerprint of Younger Dryas cooling and warming in eastern North America. *Geophysical Research Letters* **47**, e2020GL090031 (2020).

36. J. Marsicek, B. N. Shuman, P. J. Bartlein, S. L. Shafer, S. Brewer, Reconciling divergent trends and millennial variations in Holocene temperatures. *Nature* **554**, 92 (2018).

37. P. J. Bartlein, S. P. Harrison, S. Brewer, S. Connor, B. A. S. Davis, K. Gajewski, J. Guiot, T. I. Harrison-Prentice, A. Henderson, O. Peyron, I. C. Prentice, M. Scholze, H. Seppä, B. Shuman, S. Sugita, R. S. Thompson, A. E. Viau, J. Williams, H. Wu, Pollen-based continental climate reconstructions at 6 and 21 ka: a global synthesis. *Climate Dynamics* **37**, 775–802 (2011).

38. G. M. Locosselli, R. J. W. Brienen, M. de S. Leite, M. Gloor, S. Krottenthaler, A. A. de Oliveira, J. Barichivich, D. Anhuf, G. Ceccantini, J. Schöngart, M. Buckeridge, Global tree-ring analysis reveals rapid decrease in tropical tree longevity with temperature. *Proceedings of the National Academy of Sciences* **117**, 33358–33364 (2020).

39. R. Rauschkolb, Z. Li, S. Godefroid, L. Dixon, W. Durka, M. Májeková, O. Bossdorf, A. Ensslin, J. F. Scheepens, Evolution of plant drought strategies and herbivore tolerance after two decades of climate change. *New Phytologist* **235**, 773–785 (2022).

40. J. W. Williams, J. L. Blois, B. N. Shuman, Extrinsic and intrinsic forcing of abrupt ecological change: case studies from the late Quaternary. *Journal of Ecology* **99**, 664–677 (2011).

41. M. Scheffer, S. H. Hosper, M. L. Meijer, B. Moss, E. Jeppesen, Alternative equilibria in shallow lakes. *Trends in Ecology & Evolution* **8**, 275–279 (1993).

42. M. Scheffer, S. Carpenter, J. A. Foley, C. Folke, B. Walker, Catastrophic shifts in ecosystems. *Nature* **413**, 591–596 (2001).

43. H.-B. Fredriksen, K. Rypdal, Spectral Characteristics of Instrumental and Climate Model Surface Temperatures. *Journal of Climate* **29**, 1253–1268 (2016).

44. V. M. R. Muggeo, Estimating regression models with unknown break-points. *Statistics in Medicine* **22**, 3055–3071 (2003).

45. Y. Sun, J. F. McManus, S. C. Clemens, X. Zhang, H. Vogel, D. A. Hodell, F. Guo, T. Wang, X. Liu, Z. An, Persistent orbital influence on millennial climate variability through the Pleistocene. *Nat. Geosci.* **14**, 812–818 (2021).

46. H. Cheng, R. L. Edwards, A. Sinha, C. Spötl, L. Yi, S. Chen, M. Kelly, G. Kathayat, X. Wang, X. Li, X. Kong, Y. Wang, Y. Ning, H. Zhang, The Asian monsoon over the past 640,000 years and ice age terminations. *Nature* **534**, 640–646 (2016).

47. B. N. Shuman, P. Newby, J. P. Donnelly, Abrupt climate change as an important agent of ecological change in the Northeast U.S. throughout the past 15,000 years. *Quaternary Science Reviews* **28**, 1693–1709 (2009).

48. J. W. Williams, D. M. Post, L. C. Cwynar, A. F. Lotter, A. J. Levesque, Rapid and widespread vegetation responses to past climate change in the North Atlantic region. *Geology* **30**, 971–974 (2002).

49. A. W. Seddon, M. Macias-Fauria, K. J. Willis, Climate and abrupt vegetation change in Northern Europe since the last deglaciation. *The Holocene* **25**, 25–36 (2015).

50. J. W. Williams, Variations in tree cover in North America since the last glacial maximum. *Global and Planetary Change* **35**, 1–23 (2003).

51. D. Fastovich, J. M. Russell, S. T. Jackson, J. W. Williams, Deglacial temperature controls on no-analog community establishment in the Great Lakes Region. *Quaternary Science Reviews* **234**, 106245 (2020).

52. T. Laepple, E. Ziegler, N. Weitzel, R. Hébert, B. Ellerhoff, P. Schoch, B. Martrat, O. Bothe, E. Moreno-Chamarro, M. Chevalier, A. Herbert, K. Rehfeld, Regional but not global temperature variability underestimated by climate models at supradecadal timescales. *Nat. Geosci.* **16**, 958–966 (2023).

53. R. Hébert, L. Schild, T. Laepple, U. Herzschuh, Biome- and timescale-dependence of Holocene vegetation variability in the Northern Hemisphere. *Ecology and Evolution* **13**, e10585 (2023).

54. S. T. Jackson, "Pollen and spores in Quaternary lake sediments as sensors of vegetation composition: theoretical models and empirical evidence" in *Sedimentation of Organic Particles*, A. Traverse, Ed. (Cambridge University Press, Cambridge, 1994; https://www.cambridge.org/core/books/sedimentation-of-organic-particles/pollen-and-spores-in-quaternary-lake-sediments-as-sensors-of-vegetation-composition-theoretical-models-and-empirical-evidence/DCC368064032C32E792D2BBB291EFA36), pp. 253–286.

55. H. D. Grissino-Mayer, H. C. Fritts, The International Tree-Ring Data Bank: an enhanced global database serving the global scientific community. *The Holocene* **7**, 235–238 (1997).

56. S. Zhao, N. Pederson, L. D'Orangeville, J. HilleRisLambers, E. Boose, C. Penone, B. Bauer, Y. Jiang, R. D. Manzanedo, The International Tree-Ring Data Bank (ITRDB) revisited: Data availability and global ecological representativity. *Journal of Biogeography* **46**, 355–368 (2019).

57. K. Zhu, C. W. Woodall, J. S. Clark, Failure to migrate: lack of tree range expansion in response to climate change. *Global Change Biology* **18**, 1042–1052 (2012).

58. M. Mudelsee, M. E. Raymo, Slow dynamics of the Northern Hemisphere glaciation. *Paleoceanography* **20** (2005).

59. S. R. Meyers, L. A. Hinnov, Northern Hemisphere glaciation and the evolution of Plio-Pleistocene climate noise. *Paleoceanography* **25** (2010).

595 60. Y. Liu, S. T. Jackson, S. Brewer, J. W. Williams, Assessing antiquity and turnover of
596 terrestrial ecosystems in eastern North America using fossil pollen data: A preliminary
597 study. *IOP Conf. Ser.: Earth Environ. Sci.* **9**, 012005 (2010).

598 61. G. Bond, W. Showers, M. Cheseby, R. Lotti, P. Almasi, P. deMenocal, P. Priore, H. Cullen,
599 I. Hajdas, G. Bonani, A pervasive millennial-scale cycle in North Atlantic Holocene and
600 glacial climates. *Science* **278**, 1257–1266 (1997).

601 62. B. Huntley, J. R. M. Allen, Y. C. Collingham, T. Hickler, A. M. Lister, J. Singarayer, A. J.
602 Stuart, M. T. Sykes, P. J. Valdes, Millennial climatic fluctuations are key to the structure of
603 last glacial ecosystems. *PloS one* **8** (2013).

604 63. H. Wanner, J. Beer, J. Butikofer, T. J. Crowley, U. Cubasch, J. Fluckiger, H. Goosse, M.
605 Grosjean, F. Joos, J. O. Kaplan, M. Kuttel, S. A. Muller, I. C. Prentice, O. Solomina, T. F.
606 Stocker, P. Tarasov, M. Wagner, M. Widmann, Mid- to Late Holocene climate change: an
607 overview. *Quaternary Science Reviews* **27**, 1791–1828 (2008).

608 64. M. G. Turner, W. J. Calder, G. S. Cumming, T. P. Hughes, A. Jentsch, S. L. LaDeau, T. M.
609 Lenton, B. N. Shuman, M. R. Turetsky, Z. Ratajczak, J. W. Williams, A. P. Williams, S. R.
610 Carpenter, Climate change, ecosystems and abrupt change: science priorities. *Philosophical*
611 *Transactions of the Royal Society B: Biological Sciences* **375**, 20190105 (2020).

612 65. T. M. Lenton, J. Rockström, O. Gaffney, S. Rahmstorf, K. Richardson, W. Steffen, H. J.
613 Schellnhuber, Climate tipping points — too risky to bet against. *Nature* **575**, 592–595
614 (2019).

615 66. R. R. Nemani, C. D. Keeling, H. Hashimoto, W. M. Jolly, S. C. Piper, C. J. Tucker, R. B.
616 Myneni, S. W. Running, Climate-Driven Increases in Global Terrestrial Net Primary
617 Production from 1982 to 1999. *Science* **300**, 1560–1563 (2003).

618 67. Intergovernmental Panel On Climate Change (Ipcc), *Climate Change 2022 – Impacts,*
619 *Adaptation and Vulnerability: Working Group II Contribution to the Sixth Assessment*
620 *Report of the Intergovernmental Panel on Climate Change* (Cambridge University Press,
621 ed. 1, 2023; https://www.cambridge.org/core/product/identifier/9781009325844/type/book).

622 68. D. Fastovich, Code and Data for Timescale-dependent response of vegetation to climate
623 change, version 1.0, Zenodo (2024); https://doi.org/10.5281/ZENODO.12726798.

624 69. T. Webb, S. E. Howe, R. H. W. Bradshaw, K. M. Heide, Estimating plant abundances from
625 pollen percentages: The use of regression analysis. *Review of Palaeobotany and Palynology*
626 **34**, 269–300 (1981).

627 70. O. Mottl, S. G. A. Flantua, K. P. Bhatta, V. A. Felde, T. Giesecke, S. Goring, E. C. Grimm,
628 S. Haberle, H. Hooghiemstra, S. Ivory, P. Kuneš, S. Wolters, A. W. R. Seddon, J. W.
629 Williams, Global acceleration in rates of vegetation change over the past 18,000 years.
630 *Science* **372**, 860–864 (2021).

71. A. Parnell, Bchron: Radiocarbon dating, age-depth modelling, relative sea level rate estimation, and non-parametric phase modelling. *R package version* **4** (2014).

72. A. C. Parnell, J. Sweeney, T. K. Doan, M. Salter-Townshend, J. R. M. Allen, B. Huntley, J. Haslett, Bayesian inference for palaeoclimate with time uncertainty and stochastic volatility, *Journal of the Royal Statistical Society: Series C (Applied Statistics)*. **64** (2014)pp. 115–138.

73. P. J. Reimer, W. E. N. Austin, E. Bard, A. Bayliss, P. G. Blackwell, C. B. Ramsey, M. Butzin, H. Cheng, R. L. Edwards, M. Friedrich, P. M. Grootes, T. P. Guilderson, I. Hajdas, T. J. Heaton, A. G. Hogg, K. A. Hughen, B. Kromer, S. W. Manning, R. Muscheler, J. G. Palmer, C. Pearson, J. van der Plicht, R. W. Reimer, D. A. Richards, E. M. Scott, J. R. Southon, C. S. M. Turney, L. Wacker, F. Adolphi, U. Büntgen, M. Capano, S. M. Fahrni, A. Fogtmann-Schulz, R. Friedrich, P. Köhler, S. Kudsk, F. Miyake, J. Olsen, F. Reinig, M. Sakamoto, A. Sookdeo, S. Talamo, The IntCal20 Northern Hemisphere Radiocarbon Age Calibration Curve (0–55 cal kBP). *Radiocarbon* **62**, 725–757 (2020).

74. A. G. Hogg, T. J. Heaton, Q. Hua, J. G. Palmer, C. S. Turney, J. Southon, A. Bayliss, P. G. Blackwell, G. Boswijk, C. B. Ramsey, C. Pearson, F. Petchey, P. Reimer, R. Reimer, L. Wacker, SHCal20 Southern Hemisphere Calibration, 0–55,000 Years cal BP. *Radiocarbon* **62**, 759–778 (2020).

75. S. G. A. Flantua, O. Mottl, K. P. Bhatta, V. A. Felde, T. Giesecke, S. J. Goring, E. C. Grimm, S. G. Haberle, H. Hooghiemstra, S. J. Ivory, P. Kuneš, S. Wolters, A. W. R. Seddon, J. W. Williams, Mottl et al. (2021, Science) Taxonomic harmonization tables for North America, Latin America, Europe, Asia, Africa, figshare (2021); https://doi.org/10.6084/m9.figshare.13049735.v2.

76. F. Biondi, D. M. Meko, G. Piovesan, Maximum tree lifespans derived from public-domain dendrochronological data. *iScience* **26**, 106138 (2023).

77. S. R. Meyers, "Astrochron: An R package for astrochronology" (manual, 2014); https://cran.r-project.org/package=astrochron.

78. R Core Team, "R: A language and environment for statistical computing" (manual, Vienna, Austria, 2021); https://www.R-project.org/.

79. J. C. Gower, Some distance properties of latent root and vector methods used in multivariate analysis. *Biometrika* **53**, 325–338 (1966).

80. J. T. Overpeck, T. Webb, I. C. Prentice, Quantitative interpretation of fossil pollen spectra - dissimilarity coefficients and the method of modern analogs. *Quaternary Research* **23**, 87–108 (1985).

81. M. B. Osman, J. E. Tierney, J. Zhu, R. Tardif, G. J. Hakim, J. King, C. J. Poulsen, Globally resolved surface temperatures since the Last Glacial Maximum. *Nature* **599**, 239–244 (2021).

82. D. G. Gavin, W. W. Oswald, E. R. Wahl, J. W. Williams, A statistical approach to evaluating distance metrics and analog assignments for pollen records. *Quaternary Research* **60**, 356–367 (2003).

83. T. Laepple, P. Huybers, Reconciling discrepancies between Uk37 and Mg/Ca reconstructions of Holocene marine temperature variability. *Earth and Planetary Science Letters* **375**, 418–429 (2013).

84. M. E. Mann, J. M. Lees, Robust estimation of background noise and signal detection in climatic time series. *Climatic Change* **33**, 409–445 (1996).

85. S. Coats, J. E. Smerdon, S. Stevenson, J. T. Fasullo, B. Otto-Bliesner, T. R. Ault, Paleoclimate Constraints on the Spatiotemporal Character of Past and Future Droughts. *Journal of Climate* **33**, 9883–9903 (2020).

86. S. Minobe, A 50–70 year climatic oscillation over the North Pacific and North America. *Geophysical Research Letters* **24**, 683–686 (1997).

87. D. I. Vyushin, P. J. Kushner, Power-Law and Long-Memory Characteristics of the Atmospheric General Circulation. *Journal of Climate* **22**, 2890–2904 (2009).

88. J. M. Lora, D. E. Ibarra, The North American hydrologic cycle through the last deglaciation. *Quaternary Science Reviews* **226**, 25 (2019).

89. S. A. Marcott, P. U. Clark, L. Padman, G. P. Klinkhammer, S. R. Springer, Z. Y. Liu, B. L. Otto-Bliesner, A. E. Carlson, A. Ungerer, J. Padman, F. He, J. Cheng, A. Schmittner, Ice-shelf collapse from subsurface warming as a trigger for Heinrich events. *Proceedings of the National Academy of Sciences of the United States of America* **108**, 13415–13419 (2011).

90. F. He, J. D. Shakun, P. U. Clark, A. E. Carlson, Z. Y. Liu, B. L. Otto-Bliesner, J. E. Kutzbach, Northern Hemisphere forcing of Southern Hemisphere climate during the last deglaciation. *Nature* **494**, 81–85 (2013).

91. C. Buizert, V. Gkinis, J. P. Severinghaus, F. He, B. S. Lecavalier, P. Kindler, M. Leuenberger, A. E. Carlson, B. Vinther, V. Masson-Delmotte, J. W. C. White, Z. Liu, B. Otto-Bliesner, E. J. Brook, Greenland temperature response to climate forcing during the last deglaciation. *Science* **345**, 1177–1180 (2014).

92. R. F. Ivanovic, L. J. Gregoire, A. Burke, A. D. Wickert, P. J. Valdes, H. C. Ng, L. F. Robinson, J. F. McManus, J. X. Mitrovica, L. Lee, J. E. Dentith, Acceleration of Northern Ice Sheet Melt Induces AMOC Slowdown and Northern Cooling in Simulations of the Early Last Deglaciation. *Paleoceanogr. Paleoclimatology* **33**, 807–824 (2018).

93. S. A. Marcott, T. K. Bauska, C. Buizert, E. J. Steig, J. L. Rosen, K. M. Cuffey, T. J. Fudge, J. P. Severinghaus, J. Ahn, M. L. Kalk, J. R. McConnell, T. Sowers, K. C. Taylor, J. W. C. White, E. J. Brook, Centennial-scale changes in the global carbon cycle during the last deglaciation. *Nature* **514**, 616 (2014).

94. E. Monnin, A. Indermühle, A. Dällenbach, J. Flückiger, B. Stauffer, T. F. Stocker, D. Raynaud, J.-M. Barnola, Atmospheric CO2 Concentrations over the Last Glacial Termination. *Science* **291**, 112–114 (2001).

95. S. C. Brown, T. M. L. Wigley, B. L. Otto-Bliesner, C. Rahbek, D. A. Fordham, Persistent Quaternary climate refugia are hospices for biodiversity in the Anthropocene. *Nat Clim Change* **10**, 244-+ (2020).

96. S. C. Brown, C. Mellin, J. García Molinos, E. D. Lorenzen, D. A. Fordham, Faster ocean warming threatens richest areas of marine biodiversity. *Global Change Biology* **28**, 5849–5858 (2022).

97. D. A. Fordham, F. Saltré, S. Haythorne, T. M. L. Wigley, B. L. Otto-Bliesner, K. C. Chan, B. W. Brook, PaleoView: a tool for generating continuous climate projections spanning the last 21 000 years at regional and global scales. *Ecography* **40**, 1348–1358 (2017).

98. J. R. Petit, J. Jouzel, D. Raynaud, N. I. Barkov, J.-M. Barnola, I. Basile, M. Bender, J. Chappellaz, M. Davis, G. Delaygue, M. Delmotte, V. M. Kotlyakov, M. Legrand, V. Y. Lipenkov, C. Lorius, L. PÉpin, C. Ritz, E. Saltzman, M. Stievenard, Climate and atmospheric history of the past 420,000 years from the Vostok ice core, Antarctica. *Nature* **399**, 429–436 (1999).

99. C. Barbante, J.-M. Barnola, S. Becagli, J. Beer, M. Bigler, C. Boutron, T. Blunier, E. Castellano, O. Cattani, J. Chappellaz, D. Dahl-Jensen, M. Debret, B. Delmonte, D. Dick, S. Falourd, S. Faria, U. Federer, H. Fischer, J. Freitag, A. Frenzel, D. Fritzsche, F. Fundel, P. Gabrielli, V. Gaspari, R. Gersonde, W. Graf, D. Grigoriev, I. Hamann, M. Hansson, G. Hoffmann, M. A. Hutterli, P. Huybrechts, E. Isaksson, S. Johnsen, J. Jouzel, M. Kaczmarska, T. Karlin, P. Kaufmann, S. Kipfstuhl, M. Kohno, F. Lambert, A. Lambrecht, A. Lambrecht, A. Landais, G. Lawer, M. Leuenberger, G. Littot, L. Loulergue, D. Lüthi, V. Maggi, F. Marino, V. Masson-Delmotte, H. Meyer, H. Miller, R. Mulvaney, B. Narcisi, J. Oerlemans, H. Oerter, F. Parrenin, J.-R. Petit, G. Raisbeck, D. Raynaud, R. Röthlisberger, U. Ruth, O. Rybak, M. Severi, J. Schmitt, J. Schwander, U. Siegenthaler, M.-L. Siggaard-Andersen, R. Spahni, J. P. Steffensen, B. Stenni, T. F. Stocker, J.-L. Tison, R. Traversi, R. Udisti, F. Valero-Delgado, M. R. van den Broeke, R. S. W. van de Wal, D. Wagenbach, A. Wegner, K. Weiler, F. Wilhelms, J.-G. Winther, E. Wolff, EPICA Community Members, One-to-one coupling of glacial climate variability in Greenland and Antarctica. *Nature* **444**, 195–198 (2006).

100. C. J. F. ter Braak, Canonical Correspondence Analysis: A New Eigenvector Technique for Multivariate Direct Gradient Analysis. *Ecology* **67**, 1167–1179 (1986).

Supplemental Information

Methods

Fossil Pollen Abundances and Age Depth Modeling

We estimate vegetation turnover from fossil pollen abundances stored in geologic archives, such as lacustrine sediments (*34*). Fossil pollen is a tracker of plant community composition through time, albeit with some biases and limitations. Taxonomic resolution is often to the genus level (e.g. *Picea*), though species level identification is possible (e.g. *Alnus rugosa*) for some fossil pollen morphotypes, and only family-level identification is possible for others (e.g. Poaceae). Additionally, some taxa overproduce pollen and others underproduce pollen. Pine (*Pinus*) is often overrepresented in pollen assemblages while fir (*Abies*) tends to be underrepresented (*69*). Our analyses account for these production biases by using metrics that downweigh abundant fossil pollen taxa and increase the weight of rarer taxa (e.g. squared chord dissimilarity metric). When these biases are considered and accounted for in analyses, as we do here, fossil pollen is an effective representation of the source plant community. We refer the reader to Chevalier et al. (*34*) for a comprehensive review of fossil pollen as a proxy for plant community composition.

We gathered fossil pollen abundance data from the Neotoma Paleoecology Database (*11*) in May 2022, which were included as a part of the BioDeepTime database (*12*). For this fossil pollen data aggregation, we targeted any fossil pollen record in Neotoma with at least 10 fossil pollen assemblages through time and two chronological controls for the corresponding sedimentary archive (e.g. radiocarbon dates, biostratigraphy, etc.). Our initial search was based on the site list from Mottl et al. (*70*), which compiled 1,181 high-quality fossil pollen records from Neotoma that met our requirements, but we did not temporally limit our search to 18,000 years as in Mottl et al. (*70*), which produced an additional 181 fossil pollen records, hereafter referred to as "sites". Note, however, that in Neotoma, one site-level sedimentary archive may have multiple fossil pollen records, e.g. if there are multiple cores from a lake or mire.

We created age depth models using Bchron (*71*, *72*). Bchron uses information from sparse but specific ages for depths in sedimentary archives for the sites to develop a continuous model of sedimentation from which ages at every depth can be estimated (*72*). An ensemble of possible sedimentation rates are estimated from the chronological controls to generate a posterior distribution of age-depth relationships that allows uncertainty about the age-depth relationship in a sedimentary archive to be propagated to all analyses. Age controls included radiocarbon years, varve years, biostratigraphic markers, and core-top age.

Bchron models were run with default parameters (*72*), except for the radiocarbon calibration curve, which requires a hemisphere-specific calibration to convert radiocarbon years to calendar years due to interhemispheric differences in $^{14}CO_2$ production, uptake, and reservoir effects. Sites in the Northern Hemisphere were calibrated using IntCal20 (*73*) and sites in the Southern Hemisphere were calibrated using SHCal20 (*74*). Non-radiocarbon ages were incorporated into Bchron as calendar years before 1950 with Gaussian errors. Issues such as undefined age uncertainties for Ocean Drilling Project data with biostratigraphic age controls prevented age depth models from being developed for 98 sites, which were subsequently removed.

After creating new age depth models, we harmonized the taxonomy across these sites using taxa lists from Flantua et al. (*75*). We were not able to match taxa in Flantua et al. (*75*) for 21 sites, so these sites were removed from further analyses. Of these removed sites, 16 were in Oceania and

Australia because the taxonomy harmonization lists from Flantua et al. (*75*) do not include these regions (Table S2). Lastly, one site (Foy Lake, Table S2) contained negative abundances for some fossil pollen counts and was removed from further analyses. Eight sites had issues with both chronological controls and taxonomy harmonization, therefore the final compilation of fossil pollen abundances included 1,250 datasets with good spatiotemporal coverage (Table S2). Sites span the Southern Hemisphere midlatitudes to the Northern Hemisphere arctic, with the densest sampling between 40° N and 50° N, and the least dense sampling between 20° S and 50° S (Figure S6). The Northern Hemisphere is better represented across sites than the Southern Hemisphere. Temporally, these records span 1.1 million years and are heavily concentrated in the last 20,000 years (Figure S6).

Tree Longevity Estimates

We estimated tree longevity with observations from all taxa available in the International Tree Ring Data Bank (ITRDB) (*55*, *56*). We gathered all tree ring width records and retained tree ring collections where at least one tree ring record spanned 90% of the tree-ring collection chronology, so as to minimize underestimation and overestimation of longevity (*38*). We used the longest tree ring record in a collection to estimate longevity for that collection and report the median across all collections in the main text (*76*). The spatial distribution of the ITRDB is comparable to the fossil pollen sites, which have the greatest density of tree ring width records in North America and Europe and comparatively fewer records in the Southern Hemisphere (Figure 2 (*56*)). The ITRDB lacks records in the tropics, but our median estimate of tree longevity (246 years) agrees with a compilation of tree ring width records from the tropics (*38*).

Spectral Analysis

We used Thomson's multitaper method (MTM) (*22*) to estimate power spectra of fossil pollen turnover using the *astrochron* R-package (R version 4.3.1, *astrochron* version 1.2) (*77*, *78*). MTM is a Fourier-based method that reduces spectral bias (e.g., spectral leakage) through the application of multiple orthogonal data "tapers" that weigh a time series according to Slepian functions (*22*), of which we used five 3π prolate tapers. The application of Slepian data tapers imparts several positive attributes to MTM when compared to the standard discrete Fourier transform: a reduction in spectral leakage and optimal bias protection for a specified bandwidth resolution, and leveraging of the multiple tapers to provide a statistical sample for estimation of spectral power and its uncertainty (*22*). We scale spectral estimates from MTM by energy per unit frequency to return power spectral density, hereafter referred to as the power spectrum (*9*).

We further processed the fossil pollen abundances to meet the MTM requirements of a univariate, regularly sampled time series. We addressed the requirement of a single time series by using principal coordinate analysis (PCO) (*79*) on fossil pollen dissimilarity matrices to reduce the dimensionality of the fossil pollen abundances. Pollen dissimilarity matrices were calculated for each individual time series using the squared chord distance metric (*80*). We retained the primary (PCO1) and secondary (PCO2) dimensions of variability for further analysis via MTM and presented the results from the primary dimension of variability in the main manuscript. Trends in PCO1 in fossil pollen dissimilarity for the last 50,000 years show a strong signal at the Pleistocene-Holocene transition (Figure S7), suggesting that this dimension of

vegetation turnover is linked to changes in greenhouse gasses, temperature, and other climate variables (*81*). The correspondence of PCO1 to climate is particularly well-illustrated for PCO1 time series using the squared chord distance metric (Figure S7). This is likely because the squared chord distance metric consistently outperforms other distance metrics in distinguishing between two distinct fossil pollen assemblages (*80*, *82*).

We sought to identify latitudinal differences in fossil pollen dissimilarity, for comparison with climate variables which are known to have a variance structure that varies by latitude (*9*). To that end, we multiplied PCO1 by the square root of its corresponding eigenvalue. This procedure scales PCO1 for each fossil pollen assemblage by the variance explained by that dimension, enabling an assessment of whether there are spatial patterns in fossil pollen turnover. That is, a fossil pollen assemblage where PCO1 explains a substantial amount of compositional variance will have a large eigenvalue corresponding to PCO1 and PCO1 will be up-weighted, producing high spectral energy across all frequencies. In contrast, a fossil pollen assemblage where PCO1 explains little variance will have a small eigenvalue corresponding to PCO1 and PCO1 will be down-weighted.

Even temporal sampling (i.e. identical temporal distance between all consecutive samples) is required by MTM, but this condition is rarely met by proxy data extracted from geologic archives and is not met by any of our fossil pollen sites. Therefore, we interpolated PCO1 of all fossil pollen assemblages using a linear interpolation approach adapted from Laepple and Huybers (*83*). This approach aims to determine an optimal interpolation resolution and minimize energy loss at high frequencies by comparing the PCO1 power spectra to the power spectra of a power law process where $\beta = 1$. The optimal interpolation resolution is identified when the ratio between the theoretical and empirical power spectra crosses 0.7. This approach objectively determines an optimal interpolation resolution, and includes filtering to minimize the aliasing of high frequency variance that is often present in sedimentary archives (implemented in the new *astrochron* function 'linterpLH13' and present in the Zenodo data repository (*68*)).

We estimated the power spectra of global ecological turnover by performing MTM on PCO1 for individual sites after subtracting the mean from the time series, binning spectral power by frequency, and then averaging spectral power across sites within each bin. This choice was made to avoid convoluting temporal and spatial variance in the eigenvector decomposition of the community dissimilarity matrix, as would have occurred if we considered all sites and samples together. We used a bin size of 1×10^{-5}, which equates to tens of thousands of years^{-1} near the smallest frequencies (e.g. 0.00001 years^{-1} versus 0.00002 years^{-1}) and <1 years near the largest frequencies (e.g. 0.49999 years^{-1} versus 0.50000 years^{-1}). After estimating the spectra of global vegetation turnover, we determined the continuum of global vegetation turnover for specific frequency bands using an ordinary least squares regression in log-log space (*9*, *10*). As in Huybers and Curry (*9*) and Zhu et al. (*10*), we first bin log-power into evenly spaced log-frequency bins to more uniformly weight spectral estimates, which are non-evenly distributed in log coordinates. On these binned log-power estimates, frequency is a predictor of spectral power and the resulting slope is the β exponent in the $S(f) \propto f^{-\beta}$ power law relationship (*9*, *10*).. Before calculating β, but after binning log-power by log-frequency, we determined the breakpoint locations in the log-log relationship between spectral power and frequency through piecewise linear regressions in the *segmented* R package (version 1.6.2) (*44*). We constrained segmented

regressions to identify three breakpoints (low, intermediate, and high frequencies) for fossil pollen turnover and one breakpoint for simulated temperature and precipitation. The number of breakpoints was based on prior expectations for climate (*9*, *10*) and visual inspection for fossil pollen. For vegetation turnover, β was fit across the four frequency ranges between the two identified breakpoint: (1) the lowest frequency resolved and the low frequency breakpoint, (2) the low frequency breakpoint and the intermediate frequency breakpoint, (3) the intermediate frequency breakpoint and high frequency breakpoint, and (4) the high frequency breakpoint to the highest frequency resolved. For example, if a breakpoint in the log-log relationship between spectral power and frequency was identified at 115^{-1} years^{-1}, 600^{-1} years^{-1}, and $4{,}000^{-1}$ years^{-1}, β was fit between (1) the lowest frequency resolved and $4{,}000^{-1}$ years^{-1}, (2) from $4{,}000^{-1}$ years^{-1} and 600^{-1} years^{-1}, (3) from 600^{-1} years^{-1} to 115 years^{-1}, and (4) from 115 years^{-1} to the highest frequency resolved. For temperature and precipitation, we fit β between the lowest frequency resolved and the one breakpoint identified and again from the one breakpoint identified to the highest frequency resolved.

Recently, methods for estimation of temporal scaling in time series were compared for their ability to reproduce β in synthetic paleoclimate time series with known β (*28*). In these analyses MTM emerged biased towards larger β values when evaluating the full frequency range, compared to other spectral transformation methods (*28*). However, MTM showed little bias at long timescales (greater than nine times the mean resolution), moderate bias at intermediate timescales (greater than 4 times the mean resolution), and generally outperformed competing methods such as spectral transformation from the Lomb-Scargle periodogram when β is high and the input data is irregularly sampled (*28*). Only Haar structure functions more accurately estimated β from the synthetic dataset, but the approach is limited to $-1 < \beta < 3$ (*28*) and does not allow for the identification/influence of quasiperiodic/periodic signals that may bias estimates of the spectral continuum (*84*). Additionally, MTM has seen broad use in paleoclimatology (*9*, *23*, *85*) and atmospheric sciences (*86*, *87*) for estimating β, providing baseline estimates for comparison.

TraCE-21ka

TraCE-21ka is a series of fully-coupled climate model experiments that simulate the effect of transient climate forcings of the most recent deglaciation with the Community Climate System Model, version 3 (*26*, *27*). TraCE-21ka includes transient changes in ice sheet topography, meltwater forcing, orbital configuration, and greenhouse gas concentration that matched then-current proxy reconstructions (*26*, *27*). These climate simulations have been pillars of paleoclimatological research and have undergone substantial comparisons against proxy reconstructions and generally perform well (*26*, *27*, *88–91*). Unlike proxy-based climate reconstructions, TraCE-21ka offers full fields that are annually resolved and well suited for comparison against spectral estimates from fossil pollen.

TraCE-21ka has known deficiencies such as seasonal precipitation biases in North America (*88*) and imperfect greenhouse gas and meltwater forcings (*92–94*). What's more, all climate models overestimate high frequency climate variability and underestimate low frequency climate variability at local and regional scales (*52*), but our low-pass filtering procedure (summarized below) somewhat mitigates this climate model limitation by reducing high frequency variability.

Nonetheless, TraCE-21ka remains the most comprehensive set of paleoclimatic simulations for the last deglaciation, which are widely used to assess ecological relationships to paleoclimate (*95–97*). Recently, the TraCE-21ka experiments were the first climate simulations to show a scaling break in the continuum of mean global temperature that is expected to exist given physical principles (*10*).

We averaged monthly near surface temperature (2 m) and total precipitation rate into annual averages. We sought to make direct comparisons between power spectra of simulated temperature, simulated precipitation, and vegetation turnover and degraded the TraCE-21ka climate simulation to match the spatial and temporal characteristics of the fossil pollen sites. Specifically, we subsampled TraCE-21ka spatially to get the nearest grid cell for every fossil pollen site, and applied a low-pass filter with a characteristic timescale of twice the mean resolution of the corresponding fossil pollen record to guard against aliasing of high-frequency variance (*23*, *28*). We then downsampled these low-pass filtered climate time series temporally, retaining only the years with fossil pollen data. This process produced a dataset of simulated temperature and precipitation that matched fossil pollen abundances in space and time with similar temporal characteristics (i.e. low-pass smoothing induced by sedimentation). Finally, we interpolated the simulated temperature and precipitation to a regular temporal grid using the same methodology applied to the fossil pollen data (*83*). All spectral analysis for TraCE-21ka were performed on these spatiotemporally subsampled and interpolated temperature and precipitation time series.

For subsampling of the TraCE-21ka simulations, we excluded those fossil pollen samples that were outside of the temporal coverage of TraCE-21ka. Fossil pollen sites that did not contain any fossil pollen assemblage observations within the last 21,000 years were excluded and not represented in the spectral estimates of the TraCE-21ka simulations.

To capture climate variability outside of the last 21,000 years we supplement our analysis of TraCE-21ka with two proxy records that approximate global climate variability for the last two million years. We use temperature reconstructions from the EPICA Dome C ice core in Antarctica (*28*). Temperature reconstructions from Antarctic ice cores primarily track global greenhouse gas concentrations and therefore global temperature changes (*98*). We also use global average surface temperature (GAST) reconstructions from Snyder (*30*). This estimate of GAST is based on proxy-based sea surface temperature reconstructions (SST) that are scaled to surface temperatures with a value determined by examining SST-surface air temperature differences from the Paleoclimate Modelling Intercomparison Project (PMIP) model simulations. Comparisons between GAST reconstructions, EPICA Dome C, and greenhouse gasses demonstrate that both sets of proxy records used here well approximate global climate evolution (*30*). Variations in ocean circulation emerge in EPICA Dome C oxygen isotopes (*99*), but as a second order feature imposed on greenhouse gas-controlled temperature changes. The spectral continuum of temperature variability at EPICA Dome C and global surface air reconstructions were fit between 100^{-1}-$15{,}000^{-1}$ years^{-1} (*9*) and $2{,}000^{-1}$-$100{,}000^{-1}$ years^{-1} (*10*), respectively.

Uncertainty Estimation

We quantified uncertainty in our estimates of spectral power and the spectral continuum through Monte Carlo resampling of sites and Bchron posterior age estimates. Specifically, we drew 1,000 sites from our global compilation of 1,250 sites at random and for each site we drew a single posterior age estimate for MTM. We then downsampled TraCE-21ka accordingly, as described in the *TraCE-21ka* section and then performed MTM as described in the *Spectral Analysis* section. We repeated this procedure 1,000 times, which produced an ensemble of 1,000 estimates of global spectral power, β, and break point location, for climate and fossil pollen turnover, from which we reported the median and 95% confidence interval (Figure S8-S9, Table S1). All sampling was performed using a uniform distribution without replacement. This uncertainty estimation procedure assesses the influence of age model uncertainty and site selection on the global and latitudinally averaged power spectra.

Sensitivity Tests

We assessed the sensitivity of our results to our choice of fossil pollen dimensionality reduction and power spectra estimation methods (Figure S3, S10-S12). For dimensionality reduction, we tested alternative methods to reduce fossil pollen dimensionality and also tested various community dissimilarity metrics. In these sensitivity tests we calculated community dissimilarity using the Bray Curtis and Jaccard dissimilarity metrics. We also performed correspondence analysis after square root transforming the fossil pollen assemblages, which unlike PCO, does not assume linearity (*100*). Lastly, to test the sensitivity of our analyses to fossil pollen analytical accuracy, we degraded the percent abundance fossil pollen observations to presence/absence, though the Jaccard distance metric is presence/absence based as well.

Changing the dissimilarity metric and the dimension of variability analyzed did not impact any conclusions for the low and intermediate frequency regimes. However, high β in the high frequency regime appears sensitive to the choice of dissimilarity metric for PCO. We chose to present the first dimension from PCO using the squared chord distance metric because of strong support for the efficacy of the squared chord distance metric to discriminate fossil pollen assemblages (*80*, *82*). We hypothesize that high frequency sensitivity is a product of the Bray Curtis and Jaccard dissimilarity metrics overemphasizing the influence of the most abundant and rare taxa, respectively. Correspondence analyses on square root transformed fossil pollen abundances and the squared chord distance metric more evenly weigh highly abundant and rare taxa (*80*, *82*), which causes the signal of high β to emerge at high frequencies (Figure S3, S10).

Correspondence analysis produced slightly different results for latitudinally averaged power spectra because of the scaling procedure we implement (Figure S11, S12). The eigenvalues in correspondence analyses do not indicate variance explained as they do in PCO. Rather, eigenvalues correspond to correlation coefficients between the coordinates for species in the fossil pollen assemblage (i.e. species score) and coordinates for time intervals (i.e. site score) in the ordination coordinate system. However, our scaling procedure, which assumes that eigenvalues correspond to variance explained, is incompatible with correspondence analysis. Nevertheless, we include sensitivity tests for correspondence to assess the assumption of linearity in PCO.

We also tested different methods for estimating the global spectral continuum of vegetation turnover by averaging MTM adaptive spectral power (as shown in the main manuscript), MTM spectral eigencoefficients, and β for each site. The procedure for returning a global average of spectral power by averaging eigencoefficients was nearly identical to averaging by spectral power. We first performed MTM on a single site and retained the five spectral eigencoefficients for each site that correspond to the five data tapers. We then averaged the five eigencoefficients across site by binning by frequency, as described in the *Spectral Analysis* section. We then calculated spectral power at each frequency using Equation 1, where $\hat{S}_k(f)$ is spectral power and $y_k(f)$ the eigencoefficient for the kth data taper. Since we use five data tapers, this produces five estimates of $\hat{S}_k(f)$ which we average to estimate total spectral power (*22*).

$$\hat{S}_k(f) = |y_k(f)|^2 \quad \text{(Equation 1)}$$

These estimates of total spectral power were used to estimate β. Lastly, we estimated the global continuum of vegetation turnover by directly averaging β at each site. Here, we performed MTM at each site as described in the *Spectral Analysis* section and then estimated β using an ordinary least squares regression in log-log space, retaining β at each site, not spectral power. Estimates of β were then averaged across sites resulting in a global estimate of the spectral continuum of fossil pollen turnover. These sensitivity tests were performed within the same Monte Carlo framework that we use to quantify uncertainty for the fossil pollen assemblages and TraCE-21ka climate parameters.

Estimates of the global power spectra for fossil pollen turnover are insensitive to averaging by spectral power or eigencoefficients (Figure S3, S10) except at the highest frequencies where results are the most uncertain. Results were highly sensitive to averaging by β. This is a product of our piecewise regression procedure to determine the location of breaks in the log-log fit between spectral power and frequency in the high and intermediate frequency regimes. Accurately identifying the location of breaks in β between the high and high-intermediate frequency regime requires high-resolution sampling which is present in a subset of fossil pollen assemblages (Figure S3, S10). Performing breakpoint identification on spectral power at a site level increases the weight of the more abundant lower resolution sites and reduces the weight of the less abundant high-resolution sites.

Supplemental Tables and Figures

Vegetation

	β				Breakpoint		
	High Frequency Regime	High-Intermediate Frequency Regime	Low-Intermediate Frequency Regime	Low Frequency Regime	High Frequency Regime- High-Intermediate Frequency Regime ($^{-1}$ years^{-1})	High-Intermediate Frequency Regime - Low-Intermediate Frequency Regime ($^{-1}$ years^{-1})	Low-Intermediate Frequency Regime – Low Frequency Regime ($^{-1}$ years^{-1})
Global	3.51 (3.29, 3.78)	-0.09 (-0.13, -0.04)	2.82 (2.80, 2.84)	0.83 (0.81, 0.84)	152 (150, 157)	872 (857, 881)	4,789 (4,732, 4,900)
Extra-tropics (> 23.5°)	3.14 (2.99, 3.33)	-0.18 (-0.21, -0.15)	2.92 (2.90, 2.94)	0.87 (0.85, 0.88)	159 (157, 166)	871 (857, 880)	4,732 (4,731.52, 4,731.55)
Tropics (< 23.5°)	3.81 (3.23, 4.95)	1.68 (1.49, 1.78)	1.83 (1.79, 1.87)	-1.29 (-1.36, -1.14)	211 (199, 218)	541 (529, 596)	21,366 (21,135 21,962)

1062

TraCE-21ka Near Surface Temperature (2 m)

	β		Breakpoint
	High Frequency Regime	Low Frequency Regime	High Frequency Regime - Low Frequency Regime. ($^{-1}$ years^{-1})
Global	-0.15 (-0.19, -0.11)	3.05 (3.03, 3.07)	625 (567, 631)
Extra-tropics (> 23.5°)	-0.15 (-0.18, -0.10)	3.11 (3.08, 3.13)	631 (626, 638)
Tropics (< 23.5°)	1.63 (1.49, 1.76)	3.17 (3.13, 3.21)	911 (884, 981)

1063
1064
1065
1066
1067
1068

TraCE-21ka Annual Precipitation Rate

	β		Breakpoint
	High Frequency Regime	Low Frequency Regime	High Frequency Regime - Low Frequency Regime ($^{-1}$ years^{-1})
Global	-0.61 (-0.63, -0.57)	2.57 (2.56, 2.59)	635 (631, 639)
Extra-tropics (> 23.5°)	-0.93 (-0.96, -0.91)	2.40 (2.38, 2.41)	568 (565, 572)
Tropics (< 23.5°)	0.57 (0.46, 0.71)	2.38 (2.37, 2.41)	686 (631, 702)

Table S1. Parameter estimates and corresponding 95% confidence intervals in parentheses for Figures 2 and 3. Confidence intervals were calculated by bootstrapping the median. That is, each ensemble of parameter estimates was randomly resampled and the median calculated for this random resample. This procedure was repeated 10,000 times to return a distribution of median estimates for each parameter. From this distribution of bootstrapped median estimates, we report the 2.5% and 97.5% percentiles as the 95% CI.

Table S2. (Attached as Supplementary File) The list of sites considered in this study including those that were filtered out for issues with taxonomy harmonization, data quality (negative abundances), or chronological controls that prevented developing age models.

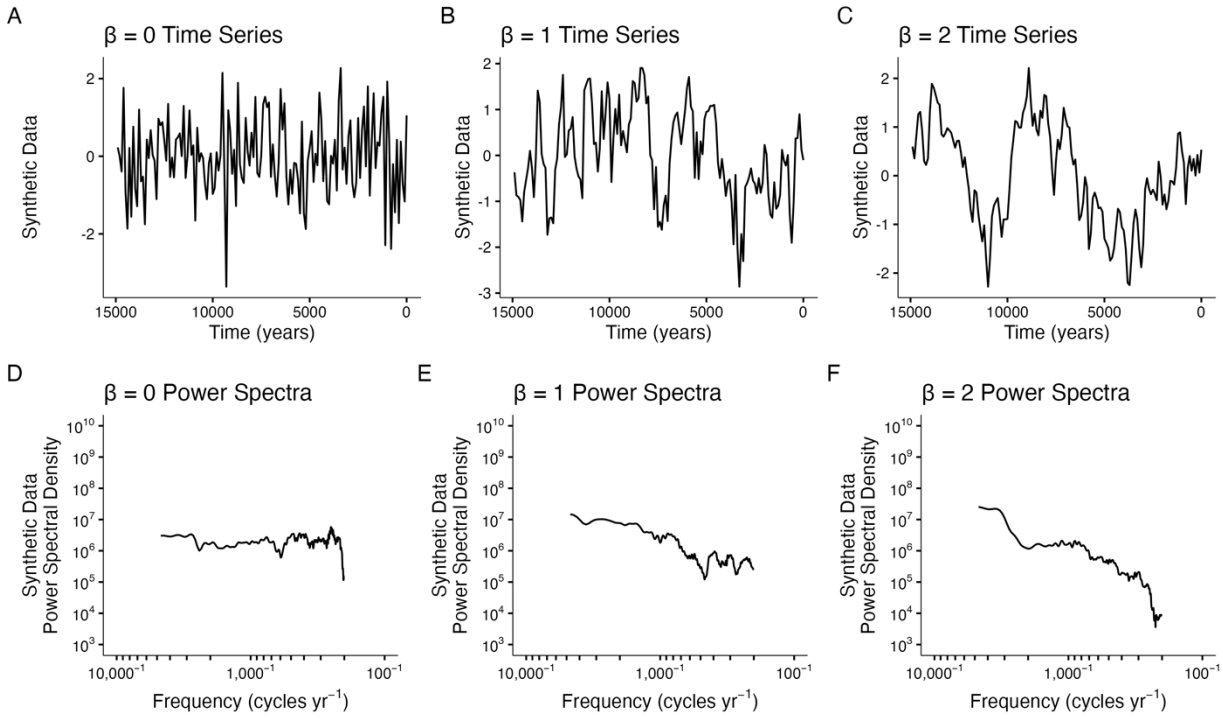

Figure S1. (A-C) Synthetic time series with a β of (A) 0, (B) 1, and (C) 2. (D-F) The corresponding power spectra for the synthetic time series in (A-C).

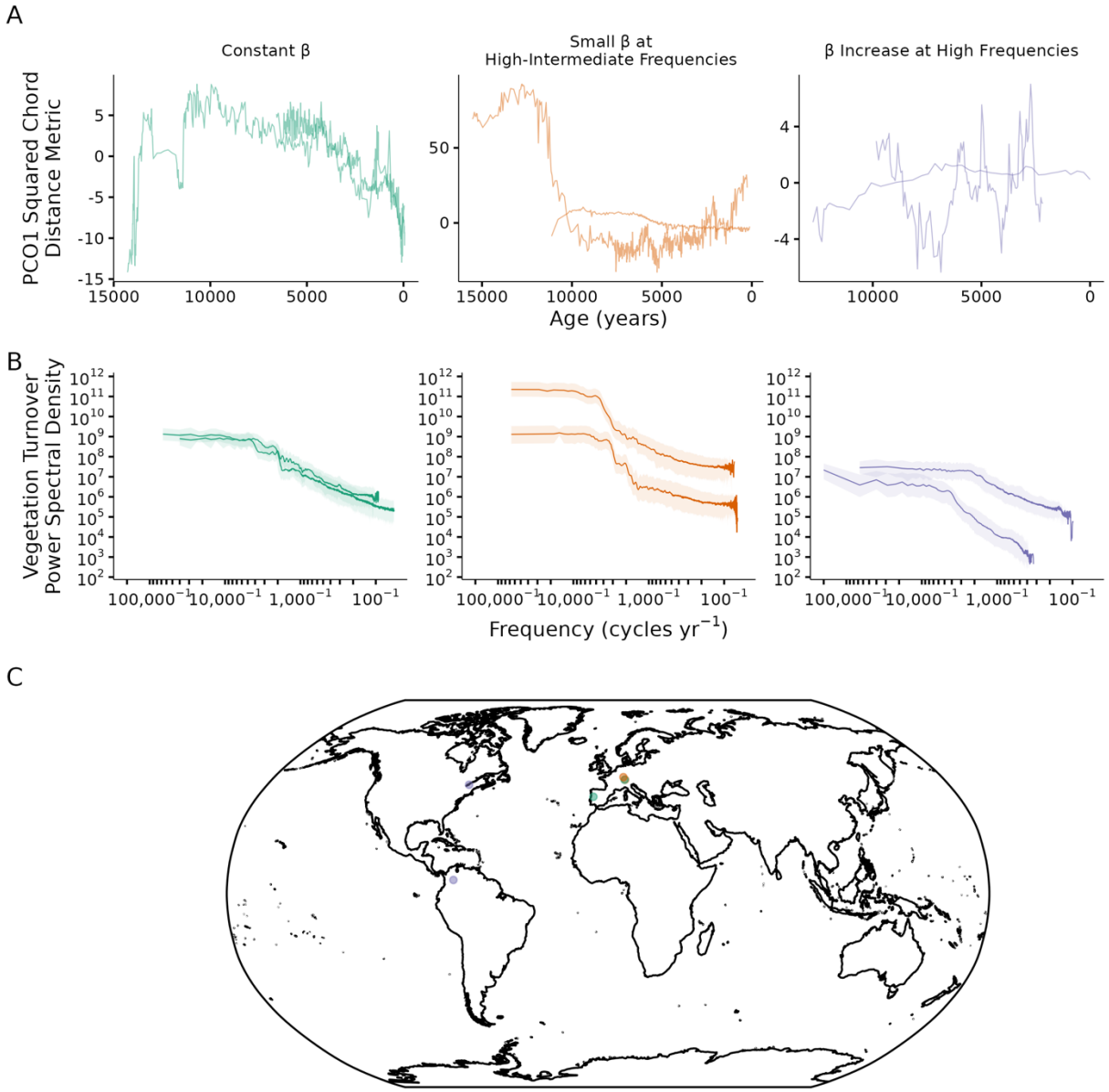

Figure S2. (A) Individual records of vegetation turnover from fossil pollen from the 1,250 site compilation that are selected to demonstrate characteristics of the global average power spectra presented in Figures 2 and 3. (B) The corresponding power spectra for the selected sites in (A). (C) A map of selected sites in (A-B). The colors correspond to different spectral characteristics that are highlighted in the main text. Green corresponds to sites that demonstrate a constant power-law scaling relationship across all frequencies and fast tracking at intermediate frequencies in the global average (872^{-1} to $4{,}789^{-1}$ years^{-1}). Orange corresponds to sites that demonstrate a break in spectral power at low-intermediate frequencies (~1,000 years^{-1}) and a small β at high-intermediate frequencies, corresponding to 152^{-1} to 872^{-1} years^{-1} in the global average spectra. Purple indicates sites that demonstrate an increase in β at the highest frequencies and corresponds to the global average spectra at frequencies higher than 152^{-1} years^{-1}. Note, all sites demonstrate a decrease in β at multimillennial timescales present in the global average at

frequencies lower than $4{,}789^{-1}$ years^{-1}. Note, in (A) the PCO1 time series are scaled by the corresponding eigenvalue, unlike in Figure S7.

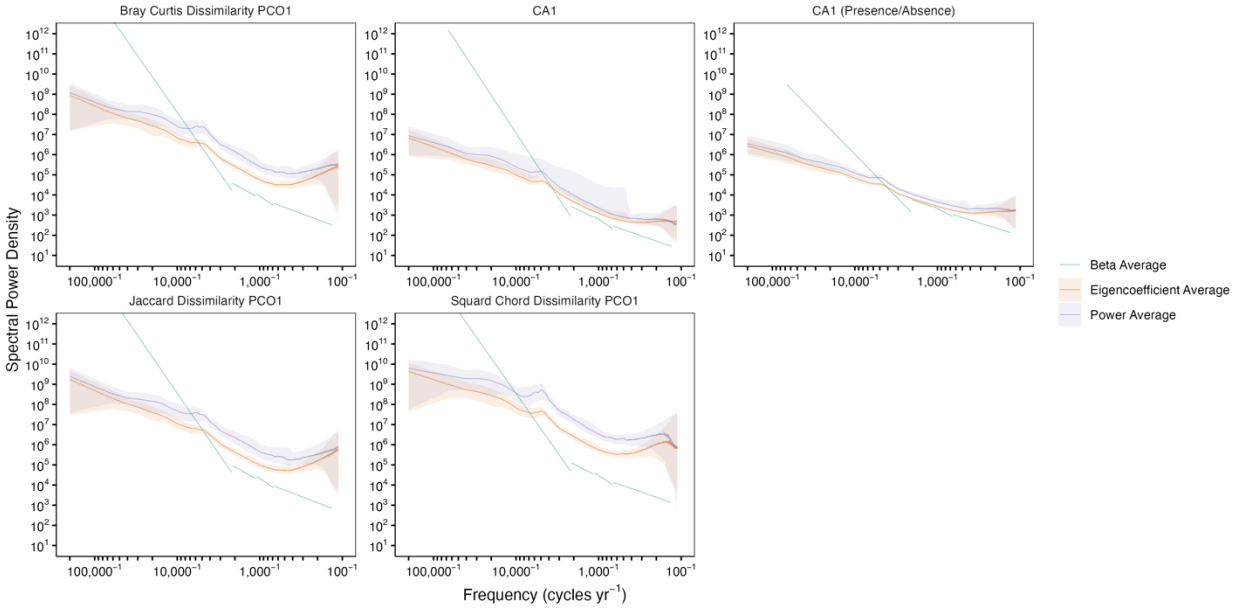

Figure S3. Sensitivity tests for the continuum of ecological variability, in which the dimensionality-reduction methods and spectral-averaging methods are altered for frequencies with spectral power estimates from a median of two sites across the ensemble of spectral power estimates. Results are presented for the primary dimension of variability from dimensionality reduction on fossil pollen assemblages. For power average, we bin by frequency and then average the spectral power values across sites. For eigencoefficient average, we bin by frequency and average the five MTM eigencoefficients corresponding to each data taper. We calculate spectral power following Equation 1. For β average, we estimate β through an ordinary least squares regression between spectral power and frequency at a single site. We then average across sites to produce a global estimate of β. This procedure only retains β, not spectral power. Therefore, for the β average method only the resulting β fit is presented. The separate lines for β average correspond to β in four frequency regimes. The breakpoint of these two lines indicates the calculated average break location averaged across sites. All sensitivity analyses were performed with the Monte Carlo resampling procedure detailed in *Uncertainty Estimation* with the shaded area corresponding to the 95% confidence interval.

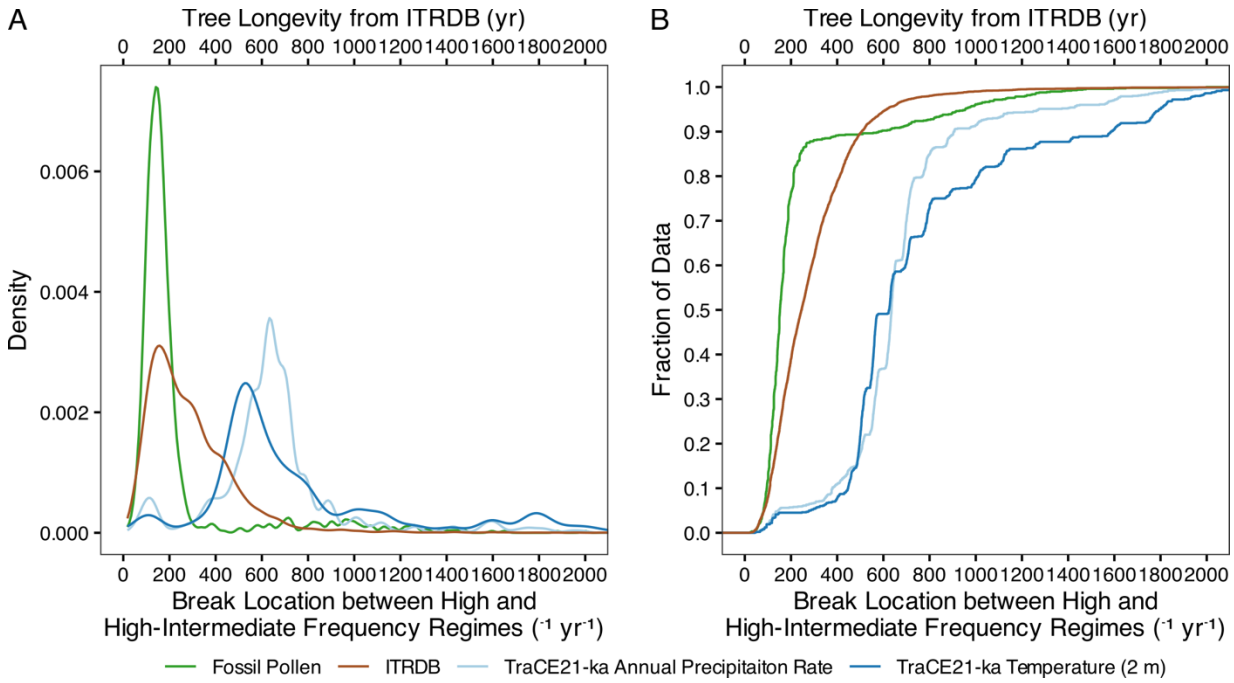

Figure S4. (A) Probability density distributions and (B) empirical cumulative distributions for the ensemble of breakpoint estimated for globally averaged power spectra between the low-intermediate and high-intermediate frequency regimes for fossil pollen (green) from our Monte Carlo resampling approach compared to tree longevity estimates from the International Tree Ring Data Bank (brown). Break locations for TraCE-21ka near-surface temperature (blue) and TraCE-21ka precipitation (light blue) correspond to one break location, previously reported (*9*, *10*), at frequencies between 100^{-1} to 1,000 $years^{-1}$. Tree longevity from the International Tree Ring Data Bank corresponds to the top horizontal axis. All pollen results presented are from PCO1 using the squared chord distance metric and averaged by spectral power.

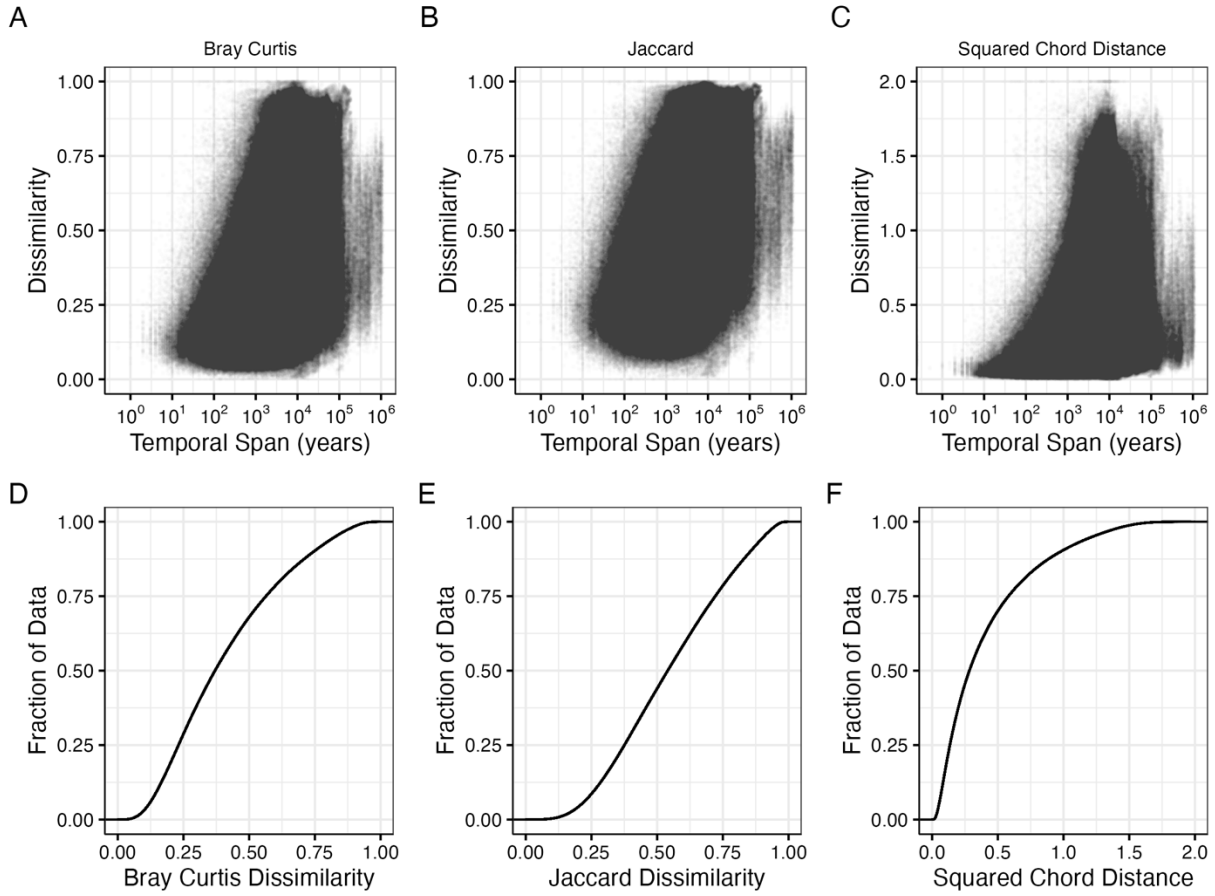

Figure S5. (A-C) Measured vegetation assemblage dissimilarity, for all sites in the global fossil pollen compilation. Dissimilarity was calculated only for assemblages from the same site and was not calculated for assemblages from different sites. Within each site, all possible pairs of fossil pollen assemblages were compared using the (A) Bray Curtis, (B) Jaccard, and (C) Squared Chord Distance metrics with the corresponding temporal span between the samples being compared retained. (D-F) The empirical cumulative distribution of all points shown in the top row of plots.

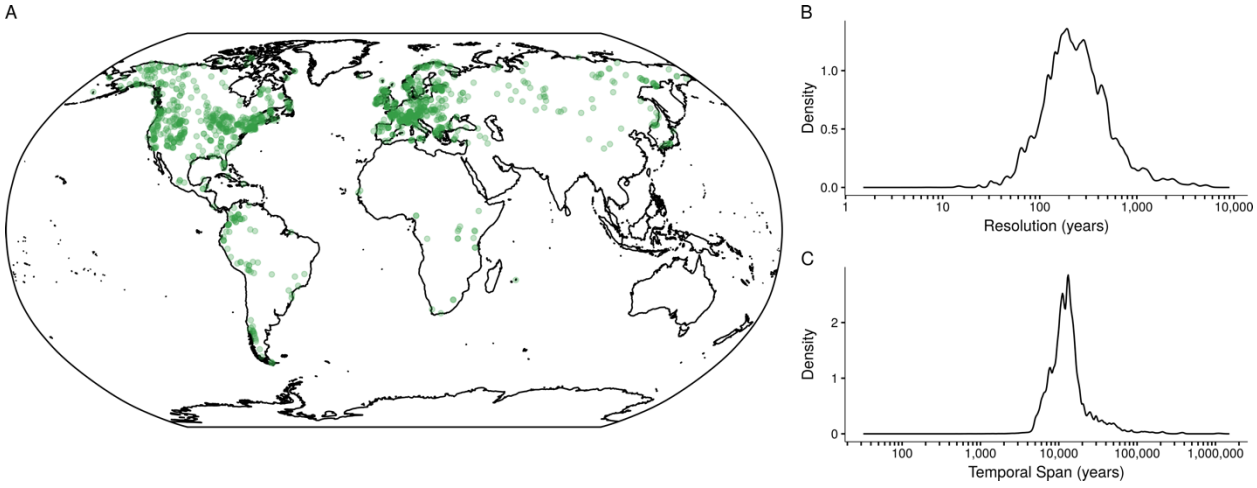

Figure S6. (A) All sites used in the spectral analyses, as in Figure 2A. The probability density of (B) temporal resolution and (C) temporal span for all sites analyzed and all corresponding posterior age estimates. Note, the Northern Hemisphere is more well represented than the Southern Hemisphere.

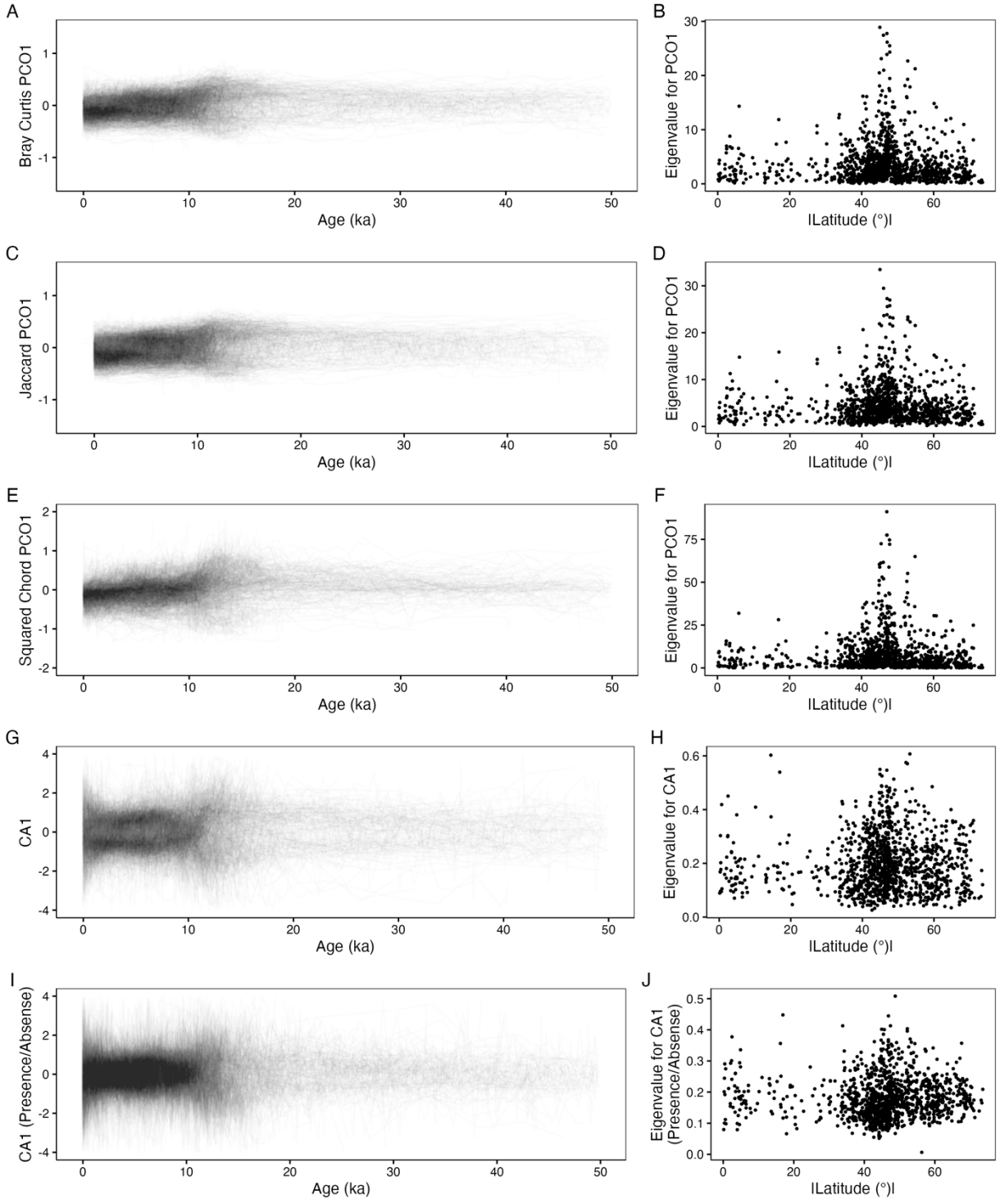

Figure S7. (A, C, E, G, I) The primary dimension of variability from 1) principal coordinates analyses (PCO) using the (A) Bray-Curtis, (C) Jaccard, and (E) Squared Chord Distance metrics

and 2) (G) correspondence analysis on fossil pollen assemblages for each site analyzed. We also performed correspondence analyses on fossil pollen assemblages after degrading the abundance observations to presence/absence (I). (B, D, F, H, J) Eigenvalues corresponding to the primary dimension of variability for each site plotted against the absolute value of the site latitude. For correspondence analyses, eigenvalues do not correspond to variance explained as they do for principal coordinate analyses. Rather, eigenvalues correspond to correlation coefficients between the coordinates for species in the fossil pollen assemblage (i.e. species score) and coordinates for time intervals (i.e. site score) in the ordination coordinate system. PCO1 using the squared chord distance metric clearly demonstrates a Pleistocene-Holocene transition. Values tend to be the most negative in the late Holocene and positive in the Last Glacial Maximum, with an abrupt change near the onset of the Holocene. For visual simplicity, the PCO1 and CA1 results for each site are unscaled by the corresponding eigenvalue. Several scaled time series are presented in Figure S2. In addition, the right column (B, D, F, H, J) demonstrates that eigenvalues tend to be higher in the high latitudes, causing PCO1 for high-latitude sites to be upscaled, producing greater total spectral power in Figure 3, relative to the low latitudes. Also for visual simplicity, we only present sites here that span the last 50,000 years, we direct readers to our Zenodo (*68*) repository where all data are present.

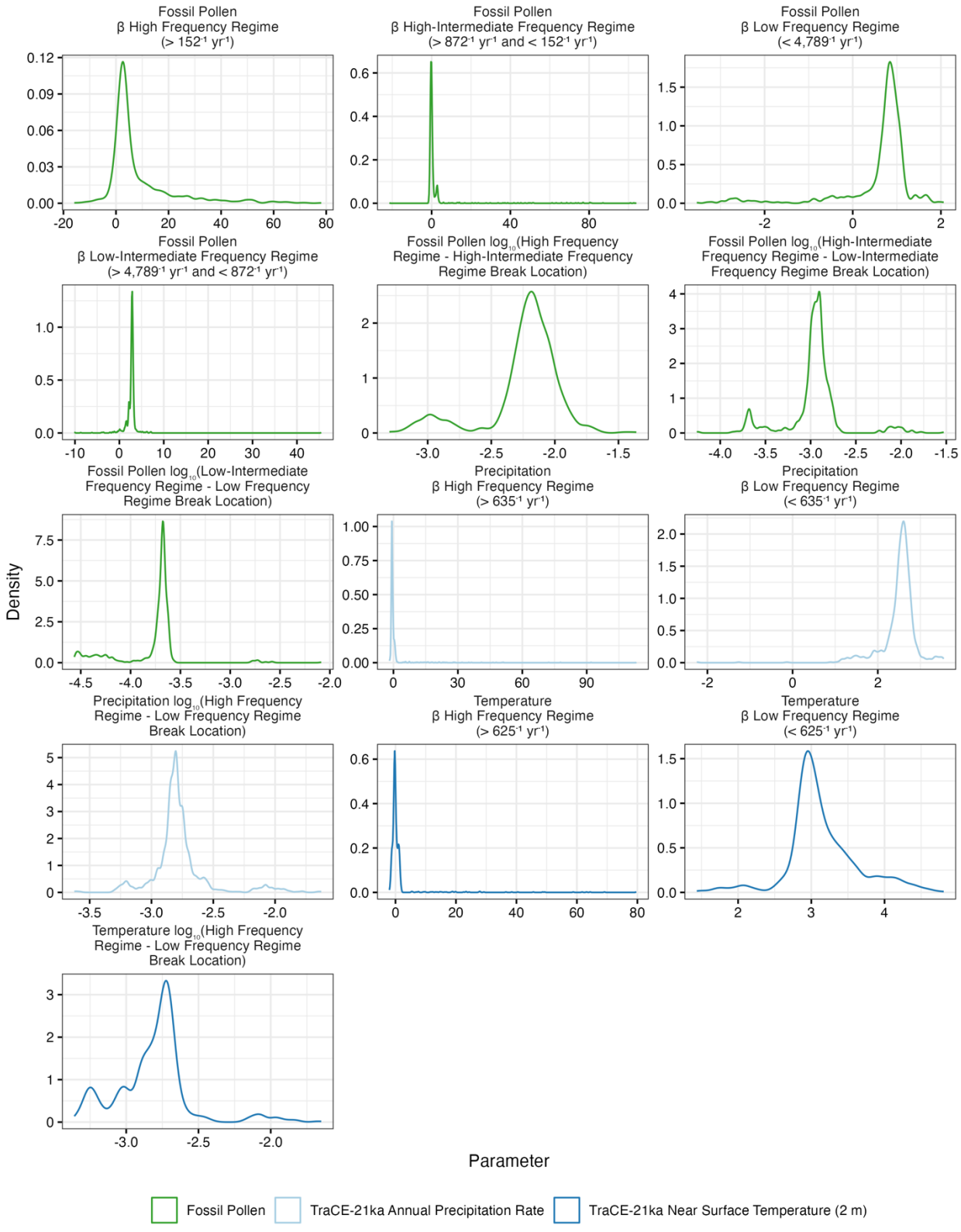

Figure S8. Each plot corresponds to the probability density function for all breakpoint and β parameter estimates in Figure 2 and Table S1. Colors correspond to parameter estimates for

fossil pollen (green), TraCE-21ka annual precipitation rate (light blue), and TraCE-21ka near surface temperature (blue).

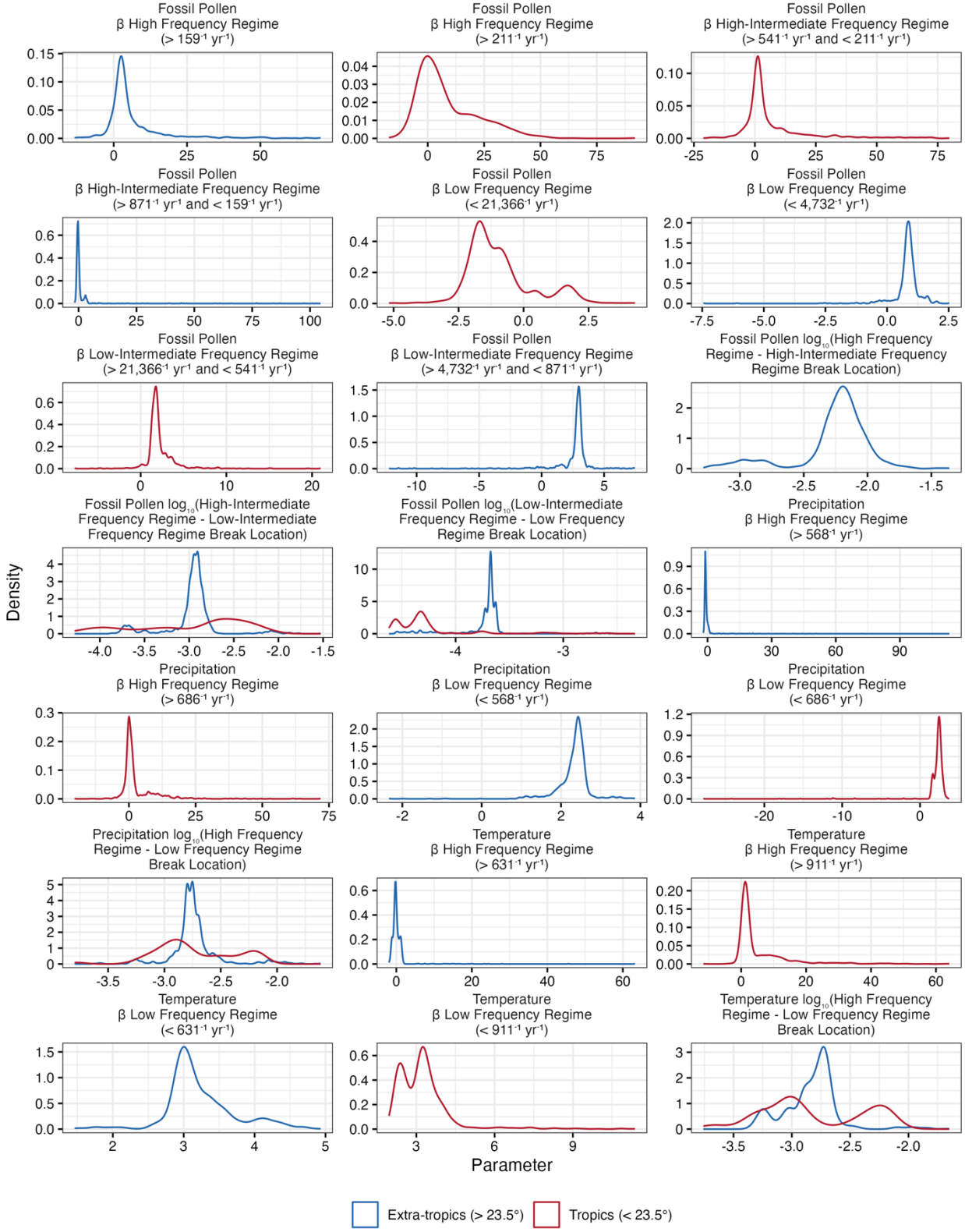

Figure S9. As in Figure S10 but for breakpoint and β estimates for Figure 3. Colors correspond to the spatial average with red indicating the tropics (< 23.5°) and blue indicating the extra-tropics (> 23.5°).

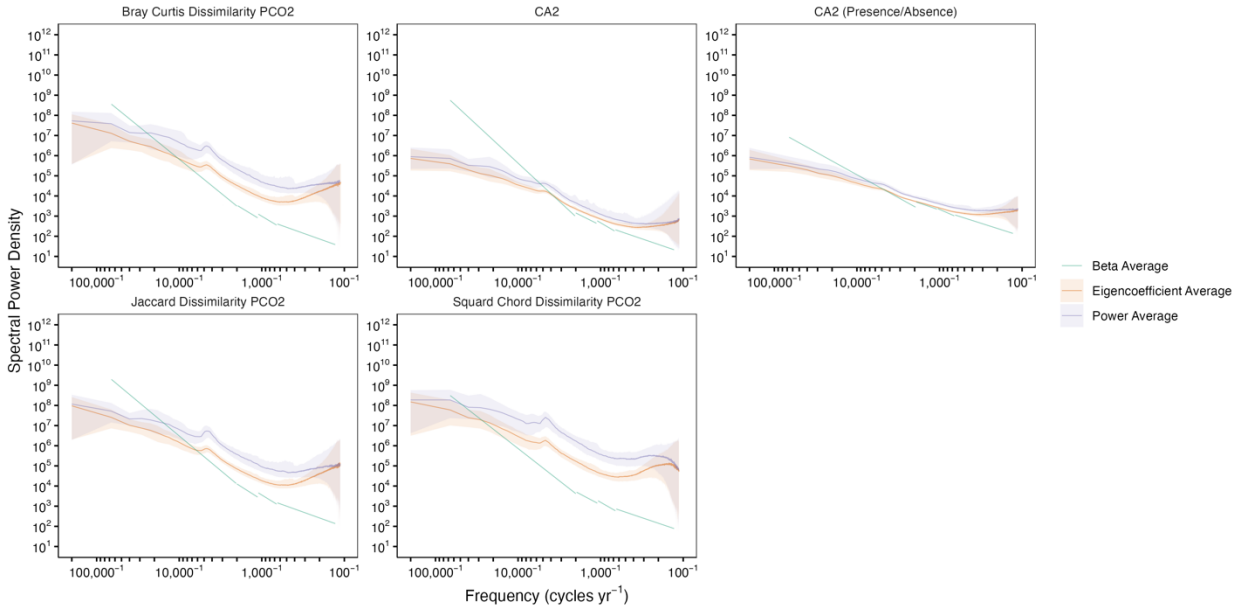

Figure S10. As in Figure S3 but for the secondary dimension of variability from dimensionality reduction on fossil pollen assemblages.

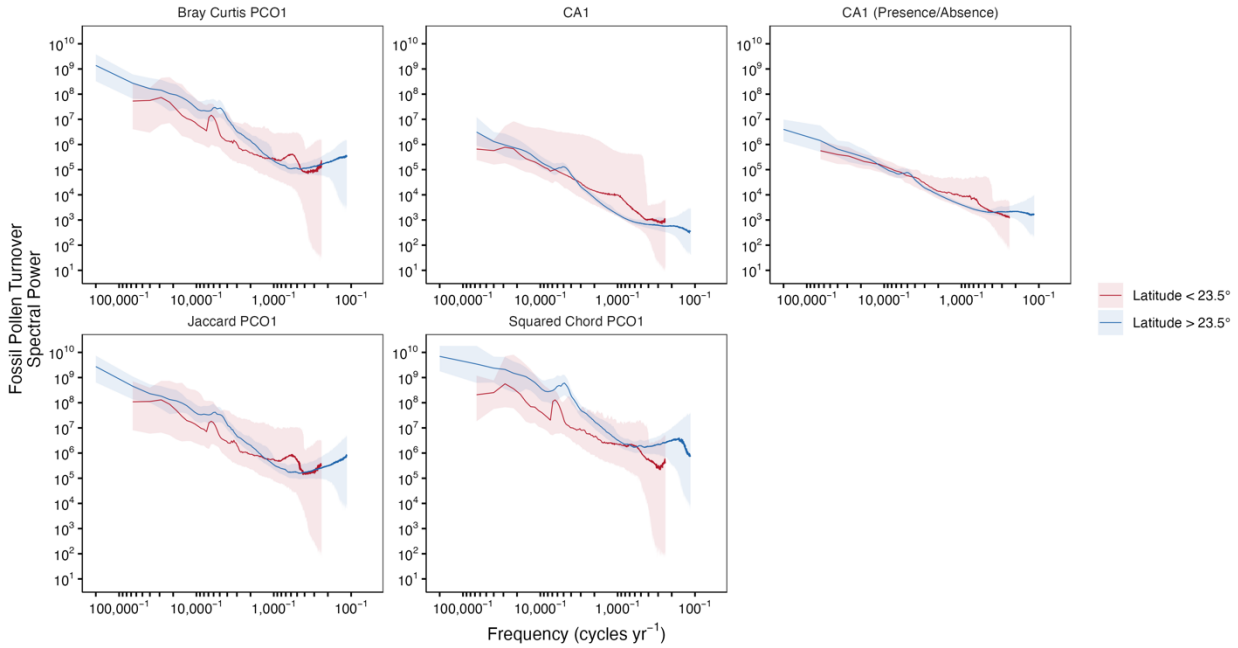

Figure S11. Sensitivity tests for latitudinal averaged power spectra for the primary dimension of variability of fossil pollen assemblages where the dimensionality reduction method is varied. All power spectra were generated by averaging spectral power after binning by frequency.

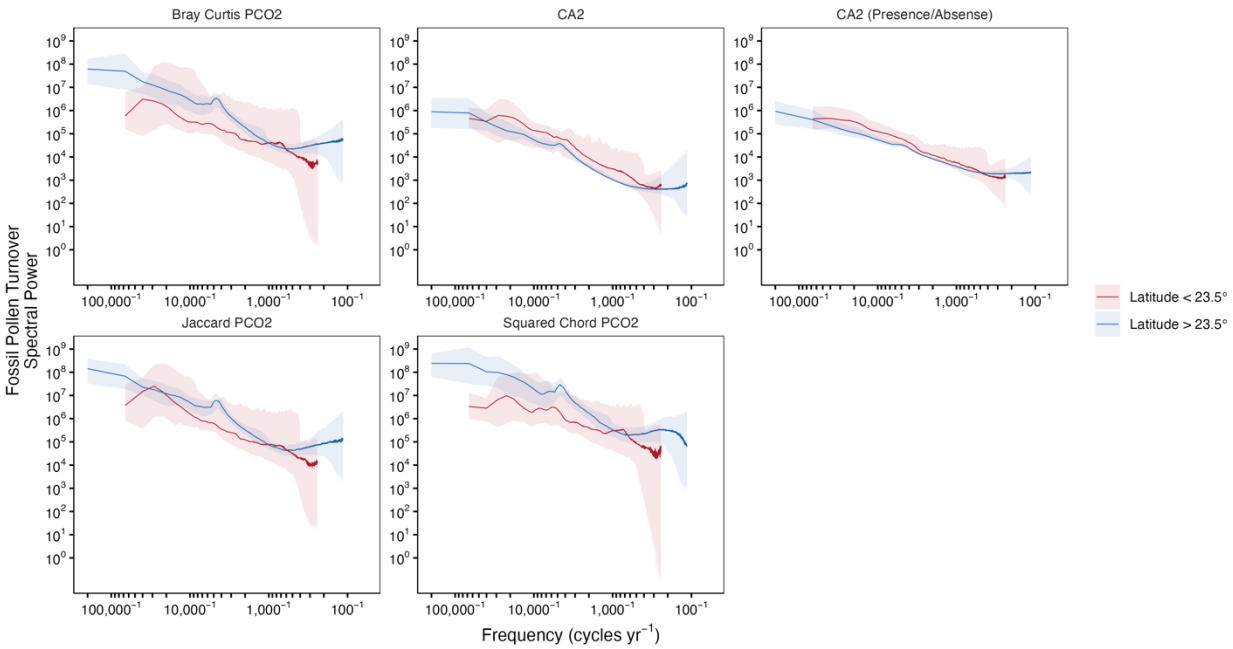

Figure S12. As in Figure S11 but for the secondary dimension of variability of fossil pollen assemblages.